Late Jurassic Magmatism and Stratigraphy in the Eastern Sakarya Zone, Turkey: Evidence for the Slab Breakoff of Paleotethyan Oceanic Lithosphere

Abdurrahman Dokuz,[1,*] *Emre Aydınçakır,*[1] *Raif Kandemir,*[2] *Orhan Karslı,*[2] *Wolfgang Siebel,*[3] *Ahmet Sami Derman,*[4,†] *and Mehmet Turan*[5]

1. Jeoloji Mühendisliği Bölümü, Gümüşhane Üniversitesi, TR29000 Gümüşhane, Turkey; 2. Jeoloji Mühendisliği Bölümü, Recep Tayyip Erdoğan Üniversitesi, Rize, Turkey; 3. Department of Geosciences, Tübingen University, 72074 Tübingen, Germany; 4. Türkiye Petrolleri A. O. Arama Dairesi, Mustafa Kemal Mah. 2. Cad. No. 86, Esentepe, 06100 Ankara, Turkey; 5. Jeoloji Mühendisliği Bölümü, Karadeniz Teknik Üniversitesi, TR61080 Trabzon, Turkey

ABSTRACT

Middle-Late Jurassic Cimmerian events in Turkey have been actively discussed in the past three decades, but proposed tectonic models associated with magmatism, metamorphism, and stratigraphic features remain controversial. To address this issue, Upper Jurassic mafic lavas are investigated at three locations (Alucra, Gümüşhane, and Olur) in the eastern Sakarya Zone, northeastern Turkey. These lavas are submarine and form planar flows parallel with the bedding plane in the Upper Jurassic carbonate sequence near the base or just below in the clastic sedimentary rocks. The basaltic lavas show calc-alkaline features and possess Nb-Ta values and Nb/U, Nb/La, and Ce/Pb ratios that are greater than those of island arc basalts. Multielement patterns are almost hump shaped, similar to ocean island basalts, which experience Pb depletion and weak negative Nb-Ta, Zr-Hf, and Ti anomalies. The low initial ($^{87}Sr/^{86}Sr$) ratios (0.70372–0.70554), positive initial ε_{Nd} values (+2.7 to +4.4), and initial Pb isotope ratios that plot between mid-ocean-ridge and ocean island basalts are consistent with a melt derived from subcontinental lithospheric mantle, metasomatized by earlier fluids from subducted sediments and plume materials from the asthenosphere. Moderate Dy/Yb ratios with an average value of 1.8 imply partial melting in the spinel-garnet transition zone at depths of ~70–100 km. Slab breakoff is suggested as a geodynamic mechanism that accounts for these geochemical signatures. This inference is also favored by stratigraphic and sedimentologic evidence from the Upper Jurassic–Lower Cretaceous sedimentary rocks, which is consistent with short-lived vertical (epirogenic) movements in the region. Lower-Middle Jurassic sequences are transgressive, suggesting that subduction-related extension opened a backarc basin (Neotethys) in the south of the Sakarya Zone. Upper Jurassic–Lower Cretaceous carbonates point tectonically to tranquility during carbonate deposition in the Neotethys Ocean, which seems to have been achieved by complete closure of the Paleotethys in the north. About 15–20 m.yr. later (Kimmeridgian), after first carbonate deposition, intraplate-type mafic lavas ascended up to the shelf surface of the Neotethys. This was followed by formation of disconformity surfaces and then accumulation of coarse clastic sediments. All this points to a short-lived epirogenic movement that we ascribe to the breakoff of the southward-subducting Paleotethyan oceanic lithosphere in the Late Jurassic.

Introduction

The Sakarya Zone (Okay and Tüysüz 1999), an elongate crustal ribbon extending from Biga Peninsula in the west to the Eastern Pontides in the east (fig. 1*a*), is one of the key areas for understanding the paleogeographic reconstruction of the Late Paleozoic and Mesozoic oceans in the Eastern Mediterranean realm. The Late Triassic–Middle Jurassic interval was dominated by the northward journey of the Sakarya Zone and subsequent collision with Laurasia. The tectonic events during this journey and collision, especially the so-called Cimmerian tectonic events, are critical to resolve the paleoreconstructions of these oceans.

Manuscript received May 7, 2016; accepted September 21, 2016; electronically published December 21, 2016.

* Author for correspondence; e-mail: dokuzabdurrahman@gmail.com.

† Deceased.

[The Journal of Geology, 2017, volume 125, p. 1–31] © 2016 by The University of Chicago. All rights reserved. 0022-1376/2017/12501-0001$15.00. DOI: 10.1086/689552

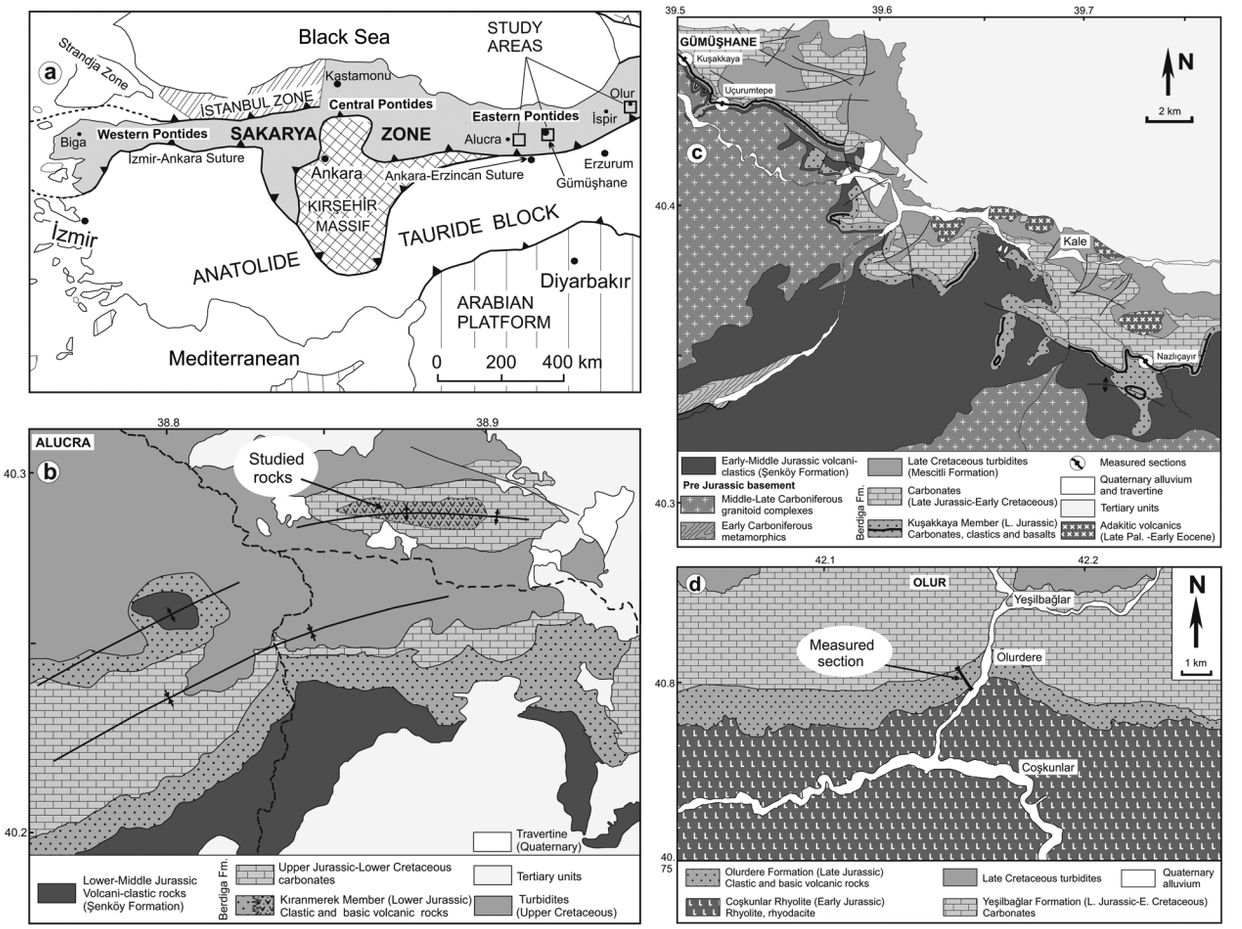

Figure 1. *a*, Main Neotethyan sutures and continental blocks of Turkey (modified from Okay and Tüysüz 1999), with locations of the study areas. *b–d*, Geological maps of the Alucra (*b*), Gümüşhane (*c*), and Olur (*d*) regions of Turkey. A color version of this figure is available online.

Two contrasting views have been suggested for the pre–Late Jurassic geographic position of the Sakarya Zone and the subduction polarity during the closure of the Paleotethys. One group of authors (Şengör and Yılmaz 1981; Görür et al. 1983; Şengör 1984; Yılmaz et al. 1997; Göncüoğlu et al. 2003; Dokuz et al. 2010) has proposed that the Sakarya Zone was once located along the northern margin of Gondwana through the Late Paleozoic. According to these authors, southward subduction of the Paleotethys during the Permian to Middle Jurassic led to the opening of several Neotethyan oceanic basins behind the terranes rifted from the northern margin of Gondwana. The İzmir-Ankara-Erzincan suture (fig. 1*a*) represents the oceanic vestiges of the northern branch of the Neotethys. The time interval that ranges from the separation of the Sakarya Zone (the westernmost terminal of the Cimmerian continent) from Gondwana (Triassic?) to the accretion of the fragment to the southern margin of Laurasia (Late Jurassic) is regarded as coeval for both the Paleotethys and the Neotethys. The Paleotethys was finally consumed in the Middle Jurassic, resulting in the collision of the Sakarya Zone with the southern margin of Laurasia. On the other hand, a second group of authors (Okay 2000; Golonka 2004; Pickett and Robertson 2004; Robertson et al. 2004; Okay et al. 2006; Ustaömer and Robertson 2010; Topuz et al. 2013) has placed the Sakarya Zone adjacent to the southern margin of Laurasia, facing a wide Tethyan Ocean in the south. According to these authors, the Tethys was formed by a number of oceanic basins that evolved episodically during Late Paleozoic to Cenozoic time. In this concept, the Paleotethys was one of these basins located to the south of the Sakarya Zone (fig. 1*a*), whereas the present Eastern

Mediterranean basin represents the final remnants of the Tethys that has not yet closed. These authors argue that the Paleotethys began to close in the Permian by northward subduction beneath Laurasia. Following a protracted period of subduction, the Paleotethys finally closed in the Paleocene, by collision of the Anatolide-Tauride Block with the Sakarya Zone, separated from the southern margin of Laurasia in the late Early Cretaceous. Ophiolitic vestiges of the İzmir-Ankara-Erzincan suture (fig. 1*a*) are accepted as representatives of this ocean.

Basaltic rocks, which occupy ~10–30-m-thick horizontal flows within the Upper Jurassic sedimentary rocks in the Alucra, Gümüşhane, and Olur areas, have been examined in this study in terms of whole-rock geochemical and Sr-Nd-Pb isotopic characteristics. The debatable issue is whether the Late Jurassic magmatism was generated in the volcanic arc of the Jurassic subduction zone along the southern margin of Laurasia or is related to the slab breakoff that is subsequent to arc-continent collision, as suggested by the Cimmerian orogeny in the Middle Jurassic. Accurate geochemical inferences from the Upper Jurassic igneous rocks together with regional tectonics contribute to the ongoing debates on the tectonic setting of the Late Jurassic magmatism in the Sakarya Zone and on the Late Paleozoic to Mesozoic reconstructions of the Paleotethys and Neotethys.

Geological Setting

The Pontides are an east-west-striking mountain chain between the Black Sea in the north and the İzmir-Ankara-Erzincan suture in the south (fig. 1*a*). From west to east, the Strandja Massif and the Istanbul and Sakarya Zones are the three terranes combined into the Pontides (Okay and Tüysüz 1999). The Eastern Pontides is a geographic name describing the easterly section of the Pontide mountain chain, which also corresponds to the eastern Sakarya Zone.

The rock sequence of the eastern Sakarya Zone can be divided into two major portions: (1) pre-Jurassic basement and (2) Mesozoic-Cenozoic cover units with igneous contributions (fig. 2). High-temperature/low-pressure quartz-feldspathic gneiss and schist as well as low- to medium-temperature amphibolite, phyllite, chert, marble, and scarce metaperidotite with Early Carboniferous metamorphic ages are the oldest rocks in the pre-Jurassic basement (Topuz et al. 2004; Okay et al. 2006; Nzegge et al. 2006; Topuz et al. 2007; Dokuz et al. 2011, 2015). Numerous small granitoids with Middle Carboniferous to Early Permian crystallization ages are situated in these metamorphic rocks throughout the Sakarya Zone (Delaloye and Bingöl 2000; Topuz et al. 2010; Dokuz 2011; Kaygusuz et al. 2012). Upper Carboniferous to Permian sediments, which unconformably overlie the basement metamorphic rocks, are preserved only in the Pulur region of the eastern Sakarya Zone (Okay and Leven 1996; Kandemir and Lerosey-Aubril 2011). A Triassic accretionary prism (the Karakaya-Küre complex), which is characterized by high-pressure/low-temperature ocean-derived rocks, is widely exposed in the central and western Sakarya Zone (Şengör 1984; Okay 2000; Pickett and Robertson 2004; Okay and Göncüoğlu 2004; Okay et al. 2006).

The Lower Jurassic Şenköy Formation (Kandemir 2004) is the first Mesozoic stratigraphic unit deposited unconformably over the heterogeneous Variscan basement (fig. 2). The Şenköy Formation is dominated by Lower Jurassic clastic sediments and pillow lavas and is accompanied by ammonitico rosso–type limestones at the bottom of the succession (Dokuz and Tanyolu 2006; Şen 2007; Kandemir and Yılmaz 2009). Felsic pyroclastics and granite porphyries (Mudurnu volcanics) have also been reported from the central and western Sakarya Zone (Genç and Tüysüz 2010). Recent works (Dokuz et al. 2006; Eyüboğlu et al. 2010; Ustaömer and Robertson 2010; Karslı et al. 2014) have described the existence of certain mafic igneous equivalents of pillow basalts, with ages varying from the Late Triassic to the Early Jurassic. The most prominent spatial feature of the formation is its highly variable thickness, for example, from 2 to 1500 m within a short distance (Kandemir 2004; Akdoğan et al. 2012). This feature was inherited from the blocky-faulted submarine topography during the deposition of sediments (Kandemir and Yılmaz 2009).

Upper Jurassic to Cenomanian carbonate-dominated sediments of the Berdiga Formation (Pelin 1977) lie conformably over the Şenköy Formation (fig. 2). However, a few places exist where pre-Jurassic basement rocks are nonconformably overlain by Berdiga Formation carbonates. Basaltic flows described in this study are observed in levels parallel to the bedding plane within the carbonates. The age of this volcanism is constrained to 155–150 Ma (Kimmeridgian) by fossils in the limestones located just below and above the basalts (Koch et al. 2008). Recent investigations reveal that commonly small granitic intrusions coeval with this basaltic volcanism are also widespread (Nzegge et al. 2006; Dokuz et al. 2010; Evcimen et al. 2014).

Cenomanian carbonates are conformably to disconformably overlain by Upper Cretaceous turbidi-

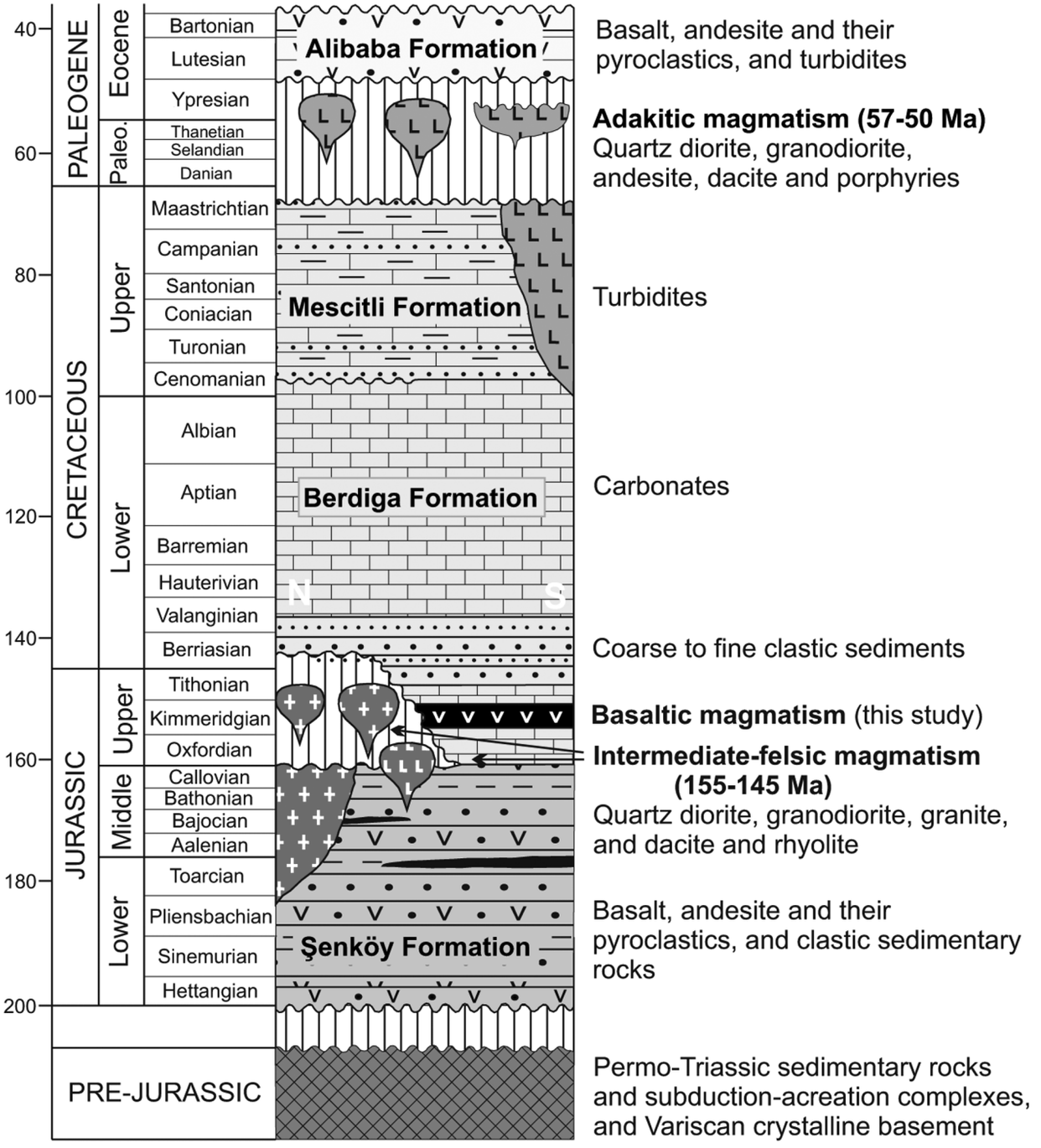

Figure 2. Mesozoic-Cenozoic stratigraphy of the southern part of the eastern Sakarya Zone. A color version of this figure is available online.

tic fan deposits of the Mescitli Formation. Toward the north, the volcanic contribution to the Mescitli Formation gradually increases and then passes to arc-type volcanics, for example, basalt, andesite, dacite, rhyolite, and, to a lesser extent, intrusive rocks, which constitute more than 60% of the entire rocks in the arc (Kaygusuz and Aydınçakır 2009; Karslı et al. 2010*b*; Aydın 2014). Lower Eocene adakitic stocks cut the Mesozoic units (Karslı et al. 2010*a*; Eyüboğlu et al. 2011; Dokuz et al. 2013; Aydınçakır 2014). Middle Eocene volcanic rocks cover unconformably both the Mesozoic units and the Lower Eo-

cene adakitic stocks (Karslı et al. 2007; Arslan et al. 2013; Aydınçakır and Şen 2013).

Upper Jurassic Stratigraphy

The Upper Jurassic–Lower Cretaceous Berdiga Formation (carbonate-dominated sedimentary rocks) is observed throughout the Sakarya Zone, although it contains lateral facies changes. In its type location (the Berdiga Mountains of Alucra, Giresun), the unit was divided into five members (Pelin 1977). In subsequent studies from different locations (e.g., Bozkuş 1992; Konak et al. 2001), the sedimentary rocks, which can be correlated with different members of the Berdiga Formation, were mapped and investigated using different names and ranks (e.g., Olurdere Formation, Yeşilbağlar Formation, and Akdağlar Limestone).

Upper Jurassic basaltic rocks have been investigated in the Alucra, Gümüşhane, and Olur areas in the eastern Sakarya Zone (fig. 1*a*). In Alucra, basaltic lavas and tuffs interbedded with clastic sedimentary rocks that lie at the succession base were termed the Kıranmerek Member (Pelin 1977). Upper Jurassic basaltic rocks along with associated sedimentary rocks in the Gümüşhane are termed the Kuşakkaya Member. In Olur, the basaltic and associated clastic sedimentary rocks having the same stratigraphic position were combined into the Olurdere Formation by Bozkuş (1992) and Konak et al. (2001). In all these locations, Upper Jurassic basaltic rocks outcrop as planar flows that are parallel to bedding in the interbedded sediments. This constrains the age of basaltic magmatism to the Kimmeridgian on the basis of index fossil findings (Koch et al. 2008). This feature also enables separation of the Late Jurassic volcanism in these locations from the Early Jurassic volcanism, which is also dominated by basalts and basaltic pyroclastics (Şen 2007).

In Alucra, basaltic rocks of the Kıranmerek Member are exposed in the core of an east-west-striking anticline of Upper Jurassic–Lower Cretaceous carbonates (fig. 1*b*; Pelin 1977). Therefore, its contact with the underlying Şenköy Formation is not observed. Sandy limestones that alternate with basaltic lithic tuffs lie at the succession base. Overlying is ~110-m-thick green basalts, including basaltic lithic tuffs (fig. 3*a*). This level is followed by ~100-m-thick sandy limestone, which alternates in places with basaltic lithic tuffs and then passes to the micritic carbonates of the Berdiga Formation.

The Upper Jurassic basaltic rocks in the Kuşakkaya Member, Gümüşhane, are exposed along a curvilinear outcrop over a large area and form a key horizon of up to 32 m thick that is traceable near the top of the Upper Jurassic Kuşakkaya Member. This basaltic level is measured and sampled at three different locations: Kuşakkaya (type location), Uçurumtepe, and Nazlıçayır (fig. 1*c*). The unit has similar lithological and stratigraphic features in all three locations. Given this similarity, the Kuşakkaya and Uçurumtepe sections are combined and illustrated in a single column in figure 3*b*.

The Uçurumtepe section of the basaltic rocks begins with a 2-m-thick basal conglomerate overlying micritic carbonates of the Kuşakkaya Member. Approximately 3-m-thick red mudstone and clays overlie in this sequence, followed by 14-m-thick massive basalts (fig. 4*a*, 4*b*). Overlying is a 2-m-thick spilitic pillow basalt including abundant vesicules later filled by calcite, chlorite, and calcedony. An ~12-m-thick second massive basalt flow overlies the pillow basalts, followed by a 0.5-m-thick succession of red mudstone and clays. A 1-m-thick upper conglomerate level, which comprises red mudstone and basalt gravels within a gray matrix, sits on a paraconformity and then grades into micritic limestones of the Berdiga Formation. The studied rocks at the Kuşakkaya section exhibit similar stratigraphic features. The only difference is the absence of lower and upper conglomerate levels.

In the Nazlıçayır section 26 km southeast of Gümüşhane (fig. 3*c*), massive basalts directly overlie gray micritic carbonates (fig. 4*c*, 4*d*). Fifteen meters above the base, these massive basalts grade into ~1–1.5-m-thick spilitic pillow basalts. Arc-shaped carbonate layers that are 1–6 cm thick also envelope these pillows. Overlying is a second massive basalt flow ~12 m thick that is followed by a 20-cm-thick red mudstone. This is overlain by gray micritic limestones. Unlike in other areas in Gümüşhane, there is a pronounced disconformity here between upper micritic limestones and following basal conglomerates, calcrudites, and calcarenites. It is observed that channels eroded into the older micritic limestones were later filled by younger overlying clastic carbonates. Another feature marks this subaerial erosion is the variations in the thickness of underlying micritic limestones bottomed by basaltic flow.

The Upper Jurassic basaltic rocks in the Olur area are observed in the Olurdere Formation (Bozkuş 1992), which stratigraphically corresponds to the Kıranmerek Member of the Berdiga Formation (fig. 1*d*; Pelin 1977). Apart from some differences in thicknesses, the sratigraphic sequence for basaltic rocks is similar to that of the Gümüşhane region. However, as shown in figure 3*d*, an important dif-

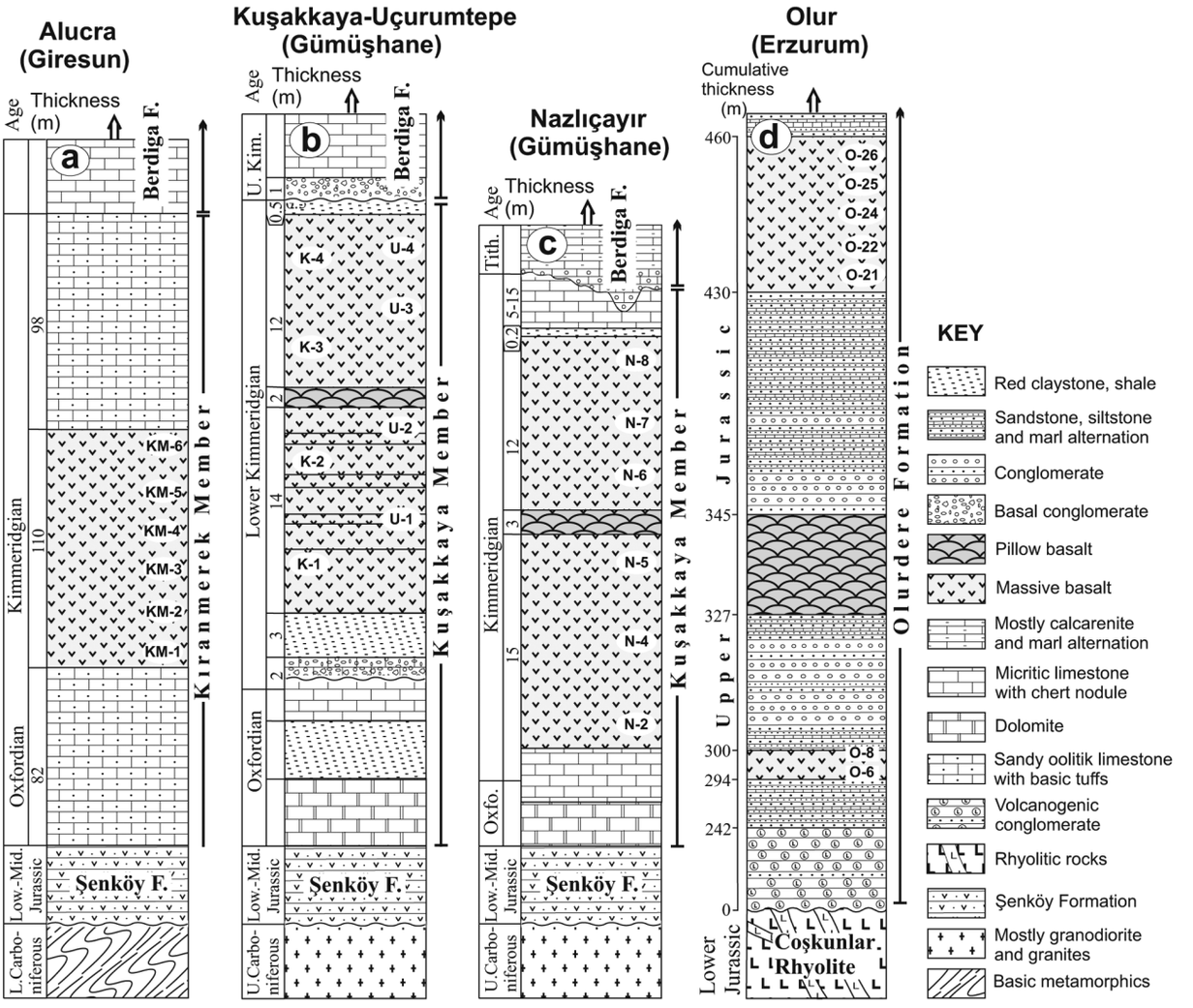

Figure 3. Columnar sections of the Alucra (*a*), Gümüşhane (*b*, *c*), and Olur (*d*) regions showing the stratigraphic positions of the Upper Jurassic basalts. A color version of this figure is available online.

ference is that clastic sediments that reach up to 85 m thick were deposited before and after the pillow basalt level.

Petrography

All the samples collected in this study are dark green to black in hand specimen. Needle-shaped plagioclase crystals are visible to the naked eye. The primary mineral assemblage identified is plagioclase + clinopyroxene + biotite + Fe-Ti oxides. The lack of olivine and amphibole in this mineral assemblage is a result of the alteration. Chlorite + sericite + Fe-Ti oxides + iddingsite ± tremolite ± calcite are the secondary minerals. Plagioclase and clinopyroxene are the dominant primary silicate phases. All the samples are characterized by an ophitic texture, but transition from ophitic texture to poikilitic texture is also widespread in the Olurdere and Kuşakkaya samples.

Plagioclase grains display two different phases: (1) phenocrysts that exhibit strong zonation and include biotite and clinopyroxe inclusions and (2) plagioclase laths, along with clinopyroxene, which form an ophitic texture (fig. 5*a*). Replacement with fine white micas (sericitization) is common. Clinopyroxene is the second common silicate phase after plagioclase. Compared with other ferromagnesian minerals, clinopyroxene is largely fresh and displays a poikilic texture (fig. 5*b*). However, alteration to chlorite, actinolite, and Fe-Ti oxides is also observed in certain thin sections. Biotite is traced as small tabular brown crystals and presents in places a corona texture with hornblende, which later completely

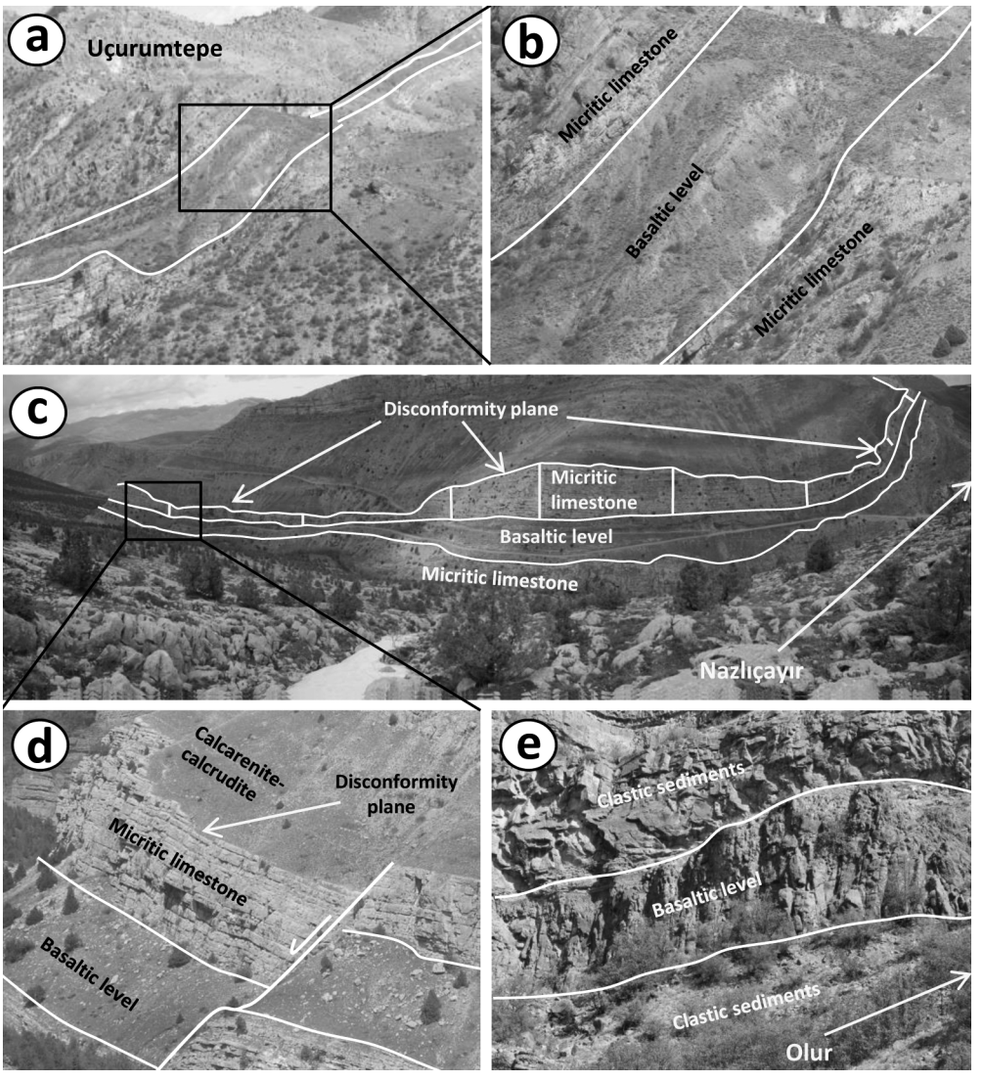

Figure 4. Field photographs of the Upper Jurassic basaltic levels and associated rocks. *a*, Appearance of the Upper Jurassic basalts as a level within the Upper Jurassic carbonates; locality, Uçurumtepe. *b*, Close-up view of the basaltic level. *c*, Panoramic photograph from Nazlicayır (Gümüşhane) showing the Upper Jurassic basaltic level and a disconformity plane (uppermost solid line) that developed between micritic limestones and clastic carbonates. *d*, Closer view of the basaltic level and disconformity plane in *c*. *e*, View of the Upper Jurassic basaltic level within the clastic rocks; locality, Olur (Erzurum). A color version of this figure is available online.

alters to chlorite (fig. 5*c*). Biotite is altered to Fe-Ti oxides along the rims and cleavages, but rarely to chlorite. Amphibole is a primary silicate phase of these rocks but is later completely replaced by chlorite and actinolite. This phase is inferred by the presence of chlorite clusters that preserve the euhedral shape of the primary amphibole and biotite crystals that envelope some of these chlorite clusters (corona texture). Although olivine is the other primary silicate phase, it was entirely transformed into brown iddingsite by subsolidus alteration (fig. 5*d*). A corona of biotite is also observed along the rims and fractures of olivine.

Chlorite is the most abundant alteration mineral that occurs during low-temperature transformation, after hornblende and rare olivine and biotite. Sericite less commonly formed after plagioclase. Iddingsite forms oval grain aggregates after olivine phenocrysts. Secondary Fe-Ti oxide occurs as anhedral grains after a partial or entire replacement of biotite and olivine.

Analytical Techniques

Twenty-seven samples were selected from the collected samples of basaltic suites for geochemical

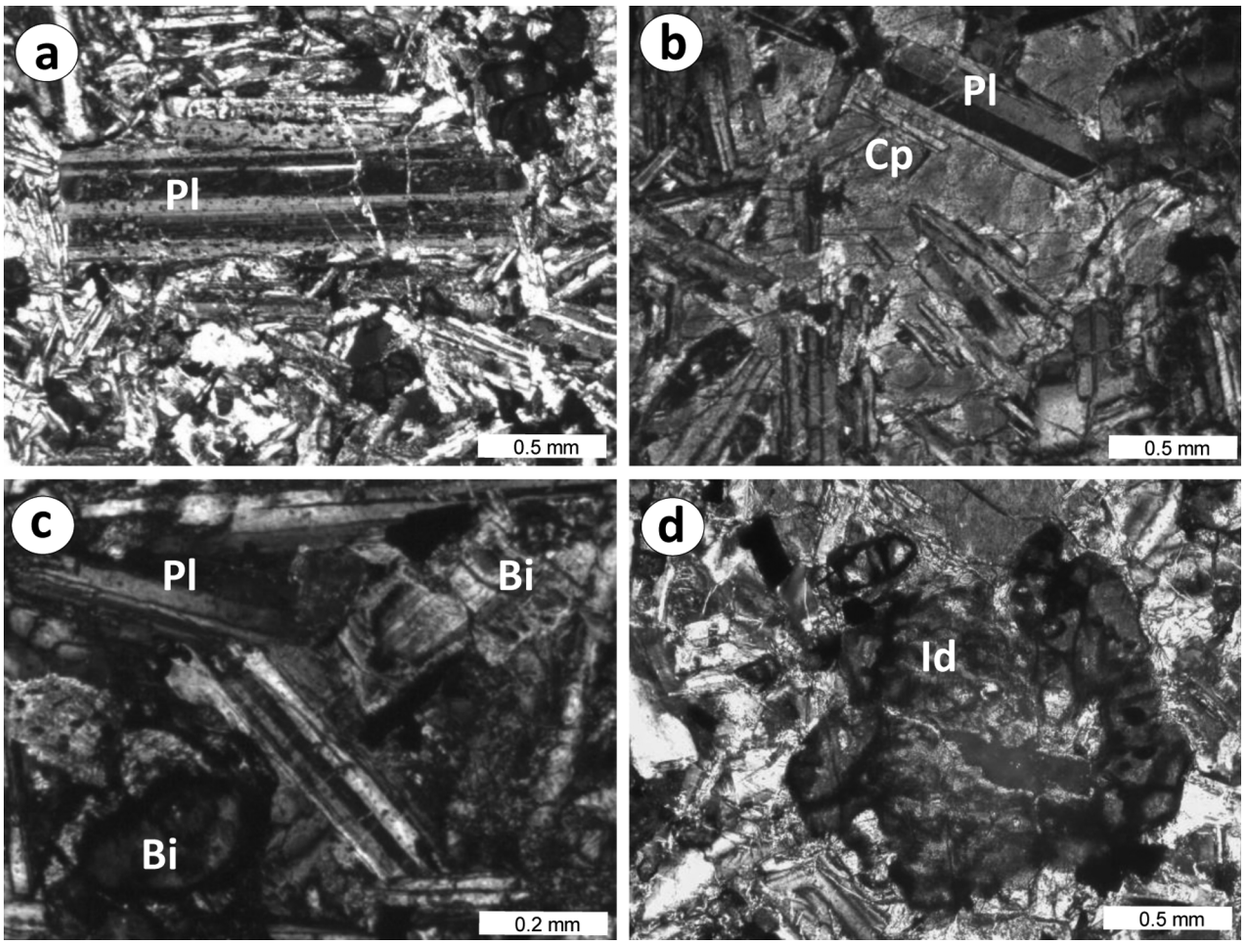

Figure 5. Photomicrographs showing the mineralogical mode and ophitic texture of the Upper Jurassic basalts. *a*, Plagioclase (Pl) porphyre within a matrix of plagioclase lath, clinopyroxene, and Fe-Ti oxide. *b*, Clinopyroxene (Cp) and plagioclase (Pl) lath. *c*, Biotite (Bi) and plagioclase (Pl). *d*, Iddingsite (Id) transformed after olivine. A color version of this figure is available online.

analyses (major and trace elements). Whole-rock major and trace element concentrations were determined at the commercial ACME Laboratories in Vancouver, Canada. Rock samples were crushed in steel crushers and ground in an agate mill to a grain size of less than 200 mesh. Major elements were obtained by inductively coupled plasma (ICP) atomic emission spectroscopy after fusion with $LiBO_2$, with detection limits of ~0.001%–0.04%. Trace elements were determined by ICP mass spectrometry after acid decomposition (5% HNO_3). STD SO-17 was certified in house against 38 certified reference materials, including CANMET SY-4 and USGS AGV-1, G-2, GSP-2, and W-2.

Sr, Nd, and Pb isotopic compositions were measured on a Finnigan MAT 262 multicollector mass spectrometer at the Department of Geosciences, Tübingen University. For Sr-Nd isotopic analyses, ~50 mg of whole-rock powder was decomposed in 52% hydrogen fluoride for 4 d at 140°C in steel-jacketed Teflon vessels. Digested samples were dried and redissolved in 6 N HCl, dried again, and redissolved in 2.5 N HCl. Sr and Nd were separated by conventional ion-exchange techniques, and their isotopic compositions were measured on single-W and double-Re filament configurations, respectively. The isotopic ratios were corrected for isotopic mass fractionation by normalizing to $^{86}Sr/^{88}Sr = 0.1194$ and $^{146}Nd/^{144}Nd = 0.7219$. The reproducibility of $^{87}Sr/^{86}Sr$ and $^{143}Nd/^{144}Nd$ during measurement was checked by analyses of NBS 987 Sr and La Jolla Nd standards, yielding average values of 0.710235 ± 0.000015 (2 SD; $n = 3$) and 0.511840 ± 0.000008 (2 SD; $n = 5$), respectively. Total procedural blanks were 200 pg for Sr and Nd. Separation and purification of Pb were carried out on Teflon columns with a 100-μL

(separation) and 40-μL (cleaning) bed of Bio-Rad AG1-X8 (100–200 mesh) anion exchange resin using HBr-HCl ion exchange. Pb was loaded with Si gel and phosphoric acid onto a Re filament and was analyzed at ~1300°C in single-filament mode. A factor of 1‰ per atomic mass unit was applied for correction of instrumental mass bias using NBS SRM 981 as reference material. Total procedural blanks for Pb were between 20 and 40 pg. Sample reproducibility is estimated at ± 0.02, ± 0.015, and ± 0.03 (2σ) for $^{206}Pb/^{204}Pb$, $^{207}Pb/^{204}Pb$, and $^{208}Pb/^{204}Pb$ ratios, respectively.

Results

Geochemistry. As noted in the section on petrography, certain primary silicate phases are entirely altered to late-stage secondary silicate phases that are more stable at low-temperature conditions. An increase in alteration is recognized as an increase in loss on ignition (LOI) content (1.4%–5.3%) of samples (table 1). There is a proportional relationship between the LOI and the modal abundance of ferromagnesian minerals, particularly olivine and amphibole, which later entirely altered to iddingsite and chlorite, respectively. The influence of increasing LOI reduces the abundance of elements compared with the unaltered precursors of these elements. Samples with high LOI contents have less than 45% SiO_2, which is similar to those of peridotites. Samples with relatively lower LOI contents are characterized by plagioclase accumulation and contain almost no olivine, pyroxene, and amphibole. This case is observed in some of the Kıranmerek (Alucra) samples, which also possess high SiO_2 concentrations. Thus, the normalization of concentrations to a volatile-free basis can provide a reasonable approach for volatile-free abundances of major elements, but only if any later enrichment in the concentrations of these elements has not occurred. To avoid such low-temperature variations of mobile elements (such as K, Na, Ba, Rb, and Sr) in rocks, the absolute values and ratios of immobile elements are primarily used during the classification of rocks and petrological interpretations.

Major and Trace Elements. Major and trace element data for the samples are presented in table 1. The rocks display medium-K calc-alkaline character (fig. 6*a*; Peccerillo and Taylor 1976). Samples from the Kuşakkaya and Olurdere exhibit basaltic composition in the total alkali versus silica diagram (fig. 6*b*; Le Bas et al. 1986), with a SiO_2 content that ranges from 44.6 to 52.5 wt% (volatile-free basis). Samples from the Kıranmerek Member show a compositional spectrum from mafic to silicic, including basalt, basaltic andesite, and dacite (SiO_2 = 45.0–69.1 wt%). These samples are moderately to highly enriched with Ti (TiO_2 = 1.12–2.2 wt%), with MgO contents ranging between 0.25 and 9.51 wt% and a Mg number (Mg# = MgO/(MgO + Fe_2O_3 × 0.889)) ranging between 7 and 51. The rocks are classified using the ratios and absolute abundances of trace elements that are assumed to be immobile during the secondary processes to test the silica-based compositional distribution. The Kuşakkaya and Olurdere samples commonly plot in the field of calc-alkaline basalt and rarely in calc-alkaline andesite fields in the classification scheme based on Co versus Th (fig. 6*c*; Hastie et al. 2007), which has been successfully applied to volcanic rocks that suffer from metasomatic loss or alkali gains. Except for three rocks that are plotted in the island arc tholeiite and basaltic andesite fields and three rocks in the shoshonitic dacite/rhyolite field, the rest of the samples are gathered in the medium- to high-K calc-alkaline basalt field and in the basaltic andesite/andesite field near the basalt line, which agrees with the above-mentioned results.

The trace element contents of these rocks differ from those of the island arc basalts in terms of higher contents of Nb (7.5–15.2 ppm), Ta (0.4–0.9 ppm), and Zr (87–213 ppm). The element values of the four evolved samples from Kıranmerek and one sample from Olurdere are unexpectedly higher (Nb = 44–76 ppm; Ta = 2.6–4.2 ppm; Zr = 611–886 ppm). These element contents also have higher Nb/La (0.5–1.6) and Nb/U (6.8–39.9) ratios than the island arc basalts (fig. 7*a*, 7*b*; Kepezhinskas et al. 1996). The Ce/Pb (12.6–80.8) ratios are higher than those of the lower continental crust and the average continental crust (fig. 7*c*; Hofman et al. 1986). The values of the rocks are consistent with those of the ocean island basalts (OIBs) and the Nb-enriched basalts (NEBs). NEBs can be divided into three magma types on the basis of Nb/La ratios (index of crustal contamination; Kieffer et al. 2004): the low-Nb/La type (Nb/La < 0.5), which exhibits higher $(Th/Nb)_N$ (>5.8) and Ce/Nb (>1.6); the mid-Nb/La type (Nb/La = 0.5–0.8), which exhibits moderate $(Th/Nb)_N$ (0.9–3.5) and Ce/Nb (3.5–5.8); and the high-Nb/La type (Nb/La > 0.8), which presents $(Th/Nb)_N$ of 0.6–1.2 and Ce/Nb of 1.7–3.0 (Xia et al. 2013). Most of the Upper Jurassic basalts of the eastern Sakarya Zone exhibit $(Th/Nb)_N$ ratios (1.3–3.0) and Nb/La ratios (0.5–0.9) that are consistent with those of a medium NEB (fig. 7*d*).

Chondrite-normalized heavy rare earth element (HREE) patterns of the samples (fig. 8) are slightly inclined to the right, and no distinct negative Eu anomalies exist except for the four samples from the Kıranmerek Member with prominent negative

Table 1. Major (wt%) and Trace (ppm) Element Data on the Upper Jurassic Basalts from the Alucra, Gümüşhane, and Olur Regions of Turkey

	Gümüşhane													
	N-2	N-4	N-5	N-6	N-7	N-8	KS-1	KS-2	KS-4	KS-5	U-1	U-2	U-3	U-4
Major elements:														
SiO_2	45.29	44.06	45.38	43.85	45.87	45.78	49.05	49.33	50.32	48.53	48.85	48.05	45.95	47.57
TiO_2	1.73	1.61	1.66	1.50	1.61	1.59	1.39	1.38	1.28	1.37	1.38	1.40	1.15	1.49
Al_2O_3	16.57	17.25	17.22	16.83	17.28	17.22	16.67	16.52	16.33	16.24	16.33	16.88	16.34	17.03
Fe_2O_3	13.47	8.39	11.21	10.35	10.16	10.21	9.59	9.74	8.65	9.23	9.65	9.18	10.60	9.01
MgO	4.47	5.88	6.02	7.51	8.21	9.27	5.35	6.25	4.30	4.36	5.30	2.81	9.03	5.94
CaO	10.13	13.29	9.69	11.06	8.55	6.45	8.63	8.28	9.23	9.96	9.30	11.52	10.20	9.24
Na_2O	3.07	2.94	2.99	2.44	2.57	2.64	3.43	3.32	3.10	3.11	3.35	3.18	2.53	3.54
K_2O	.86	.76	.78	.59	.67	1.12	1.35	1.31	2.09	1.41	1.29	1.47	.35	.71
P_2O_5	.48	.42	.47	.42	.46	.43	.36	.36	.35	.35	.36	.37	.14	.40
MnO	.08	.09	.07	.10	.08	.08	.15	.13	.09	.09	.08	.11	.08	.16
Cr_2O_3	.03	.03	.03	.03	.03	.03	.02	.02	.02	.03	.02	.02	.05	.03
LOI	3.6	5.0	4.2	5.0	4.2	4.8	3.7	3.1	4.0	5.1	3.8	4.8	3.3	4.6
Total	99.79	99.73	99.73	99.68	99.69	99.63	99.70	99.76	99.77	99.79	99.72	99.78	99.73	99.70
Mg#	27	44	38	45	48	51	39	42	36	35	38	26	49	43
Trace elements:														
Ba	213	183	192	130	160	168	221	219	216	195	212	175	67	120
Ni	119.8	110.3	115.4	132.9	140.8	127.7	69.9	69.7	79	105.1	79	82.7	170.8	106.7
Co	37	36.4	38.1	39.3	41.2	42	33.8	35.5	26.2	36	31.5	32.9	46.6	37.2
Cs	.2	<.1	.2	<.1	<.1	.4	1.3	1.3	.7	1.6	.8	2.0	.7	1.0
Ga	16.6	16.8	17.7	15.6	15.5	16	16.2	17.3	15	15.1	15.7	15.1	14.1	15.9
Hf	3.1	3.3	3.9	3.5	3.4	3.5	4.9	4.4	4.6	3.8	4.4	4.5	2.5	4.4
Nb	11.8	11	12.5	10	11.3	10.7	15.2	14.9	13.5	10.2	14.4	13.9	3.4	14.5
Rb	12.5	10.9	11.7	6.4	7.4	13.8	36.7	34.7	36	27.2	33.4	38	6.6	12.1
Sr	493	533.1	540.1	448.3	441.9	459.5	491.6	431.7	434.8	557.8	452.9	439.4	299.1	376.6
Ta	.6	.6	.7	.5	.6	.6	.9	.9	.7	.5	.8	.8	.2	.8
Th	2.2	2.1	1.8	1.6	1.8	1.7	4.5	5.2	4.9	3	4.9	4.8	.7	3.9
U	.6	.5	.5	.4	.4	.5	1.5	1.3	1.1	1.0	1.2	1.2	.2	1.3
Pb	2.1	.9	1.7	1.4	1.6	2.0	2.0	2.1	3.0	2.0	1.9	2.0	1.1	4.5
V	227	229	242	208	197	186	174	178	164	178	177	162	195	191
Zr	155.2	144.4	157.6	130.1	136.1	144	210	203.8	185.4	151.5	190.8	192.4	86.8	192.8
Y	30	29.5	30.9	25.5	24.9	24.4	33	32.9	29.5	23.9	32	28.4	23.2	30.4
La	20.1	18.9	19.8	16.9	17.1	16.6	24	23.7	22	18.2	22.2	21.8	6.8	24.5
Ce	47.2	45	47	40.7	40.8	40.5	56.5	54.7	50.5	41.8	53.4	51.3	18.2	56.8
Pr	6.04	5.69	6.07	5.12	5.25	5.1	6.84	6.64	6.22	5.21	6.33	6.16	2.51	6.77
Nd	25.1	24	25.9	21.3	22.1	21.3	27.1	27.6	24.9	22.4	25	25.5	11.4	27.4
Sm	5.31	5.18	5.59	4.52	4.59	4.44	5.5	5.45	5.11	4.38	5.34	5.06	2.99	5.48
Eu	1.76	1.73	1.83	1.56	1.52	1.55	1.61	1.59	1.52	1.36	1.52	1.44	1.09	1.62
Gd	5.42	5.32	5.43	4.69	4.57	4.45	5.5	5.44	5.11	4.07	5.04	4.85	3.57	5.24
Tb	.9	.87	.93	.74	.78	.73	.91	.91	.85	.7	.87	.82	.63	.88
Dy	5.22	4.95	5.36	4.27	4.48	4.33	5.63	5.3	5.11	3.97	5.11	5.14	4	5.08
Ho	1.06	1.04	1.09	.92	.92	.87	1.11	1.12	1.06	.87	1.09	1.04	.89	1.05
Er	3.22	3.05	3.4	2.67	2.69	2.49	3.43	3.39	3.13	2.51	3.4	3.14	2.64	3.29
Tm	.44	.4	.42	.36	.36	.34	.48	.48	.43	.36	.45	.42	.35	.44
Yb	2.84	2.73	3.0	2.37	2.52	2.28	3.29	3.25	2.94	2.36	3.07	2.93	2.41	2.96
Lu	.45	.41	.45	.36	.35	.33	.48	.48	.45	.35	.47	.45	.37	.46

	Alucra						Olur						
	KM-1	KM-2	KM-3	KM-4	KM-5	KM-6	OP-6	OP-8	OP-21	OP-22	OP-24	OP-25	OP-26
Major elements:													
SiO_2	56.42	64.63	56.66	42.75	43.51	68.01	43.54	48.96	47.04	47.50	48.98	49.03	43.00
TiO_2	1.96	1.12	1.91	2.33	2.14	1.16	1.33	1.41	1.16	1.21	1.34	1.28	2.13
Al_2O_3	15.31	13.72	14.84	16.79	16.95	14.58	17.06	18.11	16.22	17.09	17.69	18.29	14.58
Fe_2O_3	9.59	5.98	9.52	11.87	12.36	3.88	13.22	10.29	10.16	9.40	9.39	9.14	11.35
MgO	2.08	1.15	2.03	4.16	3.35	.25	6.11	6.95	7.52	6.27	4.32	4.72	9.82
CaO	2.15	.73	2.09	11.80	11.50	.62	7.82	4.04	8.18	9.10	7.68	7.45	11.28
Na_2O	4.91	4.31	4.80	3.55	3.52	4.70	4.49	5.57	4.23	4.39	5.71	5.78	1.84
K_2O	4.21	5.28	4.01	1.13	1.15	4.92	.33	.40	.55	.53	.65	.57	1.37
P_2O_5	.69	.28	.66	.45	.46	.29	.31	.34	.37	.30	.33	.32	.73
MnO	.06	.02	.06	.14	.11	.02	.24	.13	.14	.13	.14	.13	.19
Cr_2O_3	.00	.01	.00	.01	.02	.01	.03	.01	.04	.03	.01	.02	.04
LOI	2.4	2.6	3.2	4.8	4.7	1.4	5.3	3.5	4.1	3.8	3.6	3.1	2.9
Total	99.77	99.83	99.78	99.78	99.78	99.84	99.79	99.71	99.70	99.74	99.85	99.83	99.23
Mg#	20	18	19	28	23	7	34	43	45	43	34	37	49
Trace elements:													
Ba	314	193	312	160	171	238	114	128	168	179	166	196	492
Ni	5.5	5.6	4.7	54.6	46.7	1.9	88.7	23.6	105.2	63.5	15	22.7	154.9
Co	10.1	3.6	10.4	24.1	24.2	1.4	36.8	25.9	39.7	32.7	24.3	24.6	40.8
Cs	.5	2.5	.5	.5	.2	.5	.2	.2	.6	.7	1.2	1.0	.3
Ga	25	24.2	23.4	18	17.8	25.3	18.2	18.4	16.6	17.9	19.4	18.6	17.9
Hf	14.5	20.9	14.7	3	3.5	21.3	2.7	3.1	2.4	2.3	3.2	2.5	5.1
Nb	44	64.8	43.7	7.5	8.4	68.1	11.6	12.8	10.2	10.3	12.8	10.9	42.9
Rb	85.2	105.6	84.6	13.9	9.5	95	3.0	4.5	8.5	8.2	7.3	6.8	22.3
Sr	171.9	42.3	175	463.1	492.5	53.7	325.3	385.9	481.9	561.9	392.8	518.3	932.1
Ta	2.7	3.8	2.6	.4	.5	4.0	.6	.7	.5	.6	.6	.6	2.3
Th	14.4	17.7	15.1	1.2	1.4	18.2	2.1	2.7	2.1	2.2	2.5	2.4	5.1
U	2.4	2.4	3.2	1.1	.8	2.8	.5	.6	.5	.4	.6	.5	1.6
Pb	5.8	5.4	6.7	1.6	1.4	2.0	1.2	1.2	2.5	2.2	1.8	2.8	3.5
V	62	22	59	323	325	9.0	191	210	176	193	200	183	185
Zr	611.3	833.7	616.6	124.7	132.4	885.7	98.4	107.1	86.2	83.9	107.3	92.2	213.3
Y	92	94.9	87.3	29.2	28.5	100.1	25	26.8	19.4	18.4	21.9	19.6	21.8
La	64.4	62.7	63.6	14.5	16.2	74.5	18.2	18.8	16.5	15.8	17.9	15.2	46.7
Ce	135.5	137.6	131.8	36.6	39.9	161.6	40	42.5	37.2	36	40.8	35.7	88.1
Pr	17.22	16.48	17.13	4.75	5.18	18.83	4.73	5.02	4.49	4.2	4.77	4.23	9.75
Nd	71.4	65.2	68.8	22	23.5	75.1	20.5	21	19.8	17.8	20.9	18.2	37.4
Sm	13.82	13.43	13.16	4.99	5.08	14.3	4.2	4.49	3.92	3.69	4.27	3.78	7.65
Eu	3.26	2.31	3.14	1.7	1.75	2.43	1.44	1.56	1.25	1.2	1.35	1.26	2.25
Gd	14.78	13.76	13.69	5.55	5.68	14.9	4.49	4.97	3.88	3.7	4.27	3.98	6.18
Tb	2.53	2.43	2.4	.88	.88	2.61	.72	.79	.62	.6	.69	.63	1.0
Dy	15.42	15.51	14.79	5.04	5.05	15.86	4.16	4.44	3.47	3.37	3.93	3.52	4.75
Ho	3.33	3.36	3.09	1.05	1.05	3.47	.82	.94	.72	.68	.81	.7	.81
Er	9.88	10.38	9.26	3.04	2.87	10.72	2.34	2.56	2.04	1.86	2.34	1.99	1.99
Tm	1.42	1.58	1.39	.42	.42	1.63	.32	.37	.29	.28	.34	.29	.3
Yb	9.3	10.85	9.26	2.75	2.61	10.97	1.96	2.33	1.81	1.8	2.3	1.73	1.54
Lu	1.4	1.63	1.38	.41	.41	1.68	.29	.33	.27	.26	.31	.28	.21

Note. LOI = loss on ignition; Mg# = $MgO/(MgO + Fe_2O_3 \times 0.889)$.

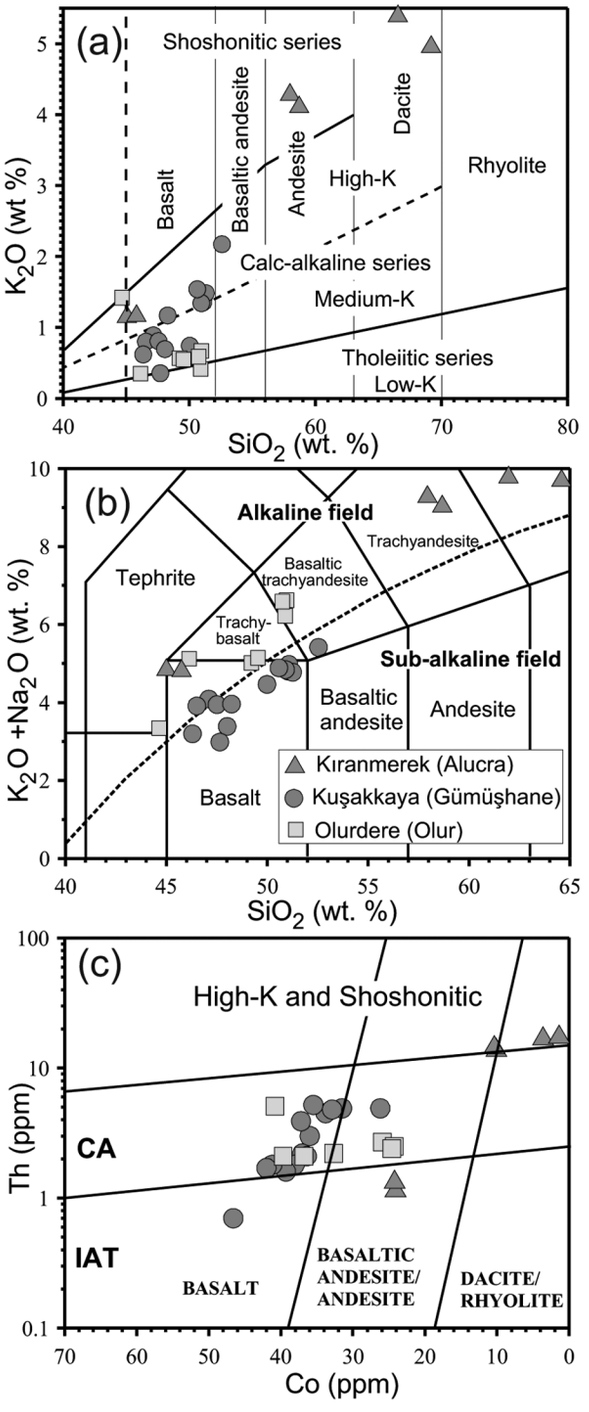

Figure 6. Various classification diagrams for the Upper Jurassic basalts from the Alucra, Gümüşhane, and Olur regions of Turkey. *a*, K_2O versus SiO_2 (wt%) diagram (Peccerillo and Taylor 1976). *b*, Total alkali versus silica diagram (Le Bas et al. 1986). *c*, Th versus Co (ppm) diagram (Hastie et al. 2007). CA = calc-alkaline; IAT = island arc tholeiite. A color version of this figure is available online.

Eu anomalies and Ba, Sr, and Ti anomalies in the multielement patterns of the samples. The primitive mantle (PM)–normalized multielement patterns of the rocks (fig. 8) resemble those of the island arc and continental arc basalts, such as negative Nb, Ta, and Ti anomalies, and enrichments in large ion lithophile elements (LILEs) compared with high field strength elements (HFSEs). However, the size of these negative anomalies diminishes in the samples from the Olurdere and in multielement patterns that are almost similar to those typical for continental rift basalts and OIBs. In addition, enrichments above 10 times chondrite are clear for all the trace elements, which differ from those of subduction-related basalts.

Sr-Nd-Pb Isotopes. Age-corrected (assuming t = 155 Ma) Sr-Nd-Pb isotope ratios of Upper Jurassic basalts are presented in table 2. As shown in the $^{87}Sr/^{86}Sr(t)$ versus $\varepsilon_{Nd}(t)$ diagram (fig. 9; Zindler and Hart 1986), the samples plot above the bulk silicate Earth value and display a very narrow range of initial $^{87}Sr/^{86}Sr$ ratios, such as from 0.70372 to 0.70418 in the Kıranmerek basalts, from 0.70422 to 0.70459 in the Kuşakkaya basalts, and from 0.70448 to 0.70554 in the Olurdere basalts. A slight increase in the initial $^{87}Sr/^{86}Sr$ isotope ratios of basalts from Kıranmerek in the west through Kuşakkaya to Olurdere in the east is apparent. All the Upper Jurassic basalts possess uniform initial ε_{Nd} values of +2.7 to +4.4. These Sr isotope ratios and ε_{Nd} values are highly comparable with those of Upper Jurassic granitoids from the Yusufeli area in the eastern Sakarya Zone (Dokuz et al. 2010), Jurassic Mudurnu volcanic rocks from the central Sakarya Zone (Genç and Tüysüz 2010), and Middle Jurassic volcanic rocks from the Kapan Zone in Armenia (Mederer et al. 2013). Basalts have initial $^{206}Pb/^{204}Pb$ ratios of 17.60–18.31, initial $^{207}Pb/^{204}Pb$ ratios of 15.52–15.60, and initial $^{208}Pb/^{204}Pb$ ratios of 37.59–38.28, which plot above the Northern Hemisphere reference line (NHRL), as defined by Hart (1984) for mid-ocean ridge basalt (MORB) and OIB from the Northern Hemisphere (fig. 10*a*, 10*b*). These Pb isotope ratios are also similar to those obtained by Mederer et al. (2013) for Middle Jurassic volcanic rocks.

Discussion

Contamination. Except for four differentiated samples from the Kıranmerek Member, the Upper Jurassic rocks are basic, with SiO_2 contents of less than 52 wt%, suggesting that the rocks are in equilibrium with their mantle source and that bulk crustal contamination is insignificant. Low initial $^{87}Sr/^{86}Sr$ and positive ε_{Nd} values are also consistent with the

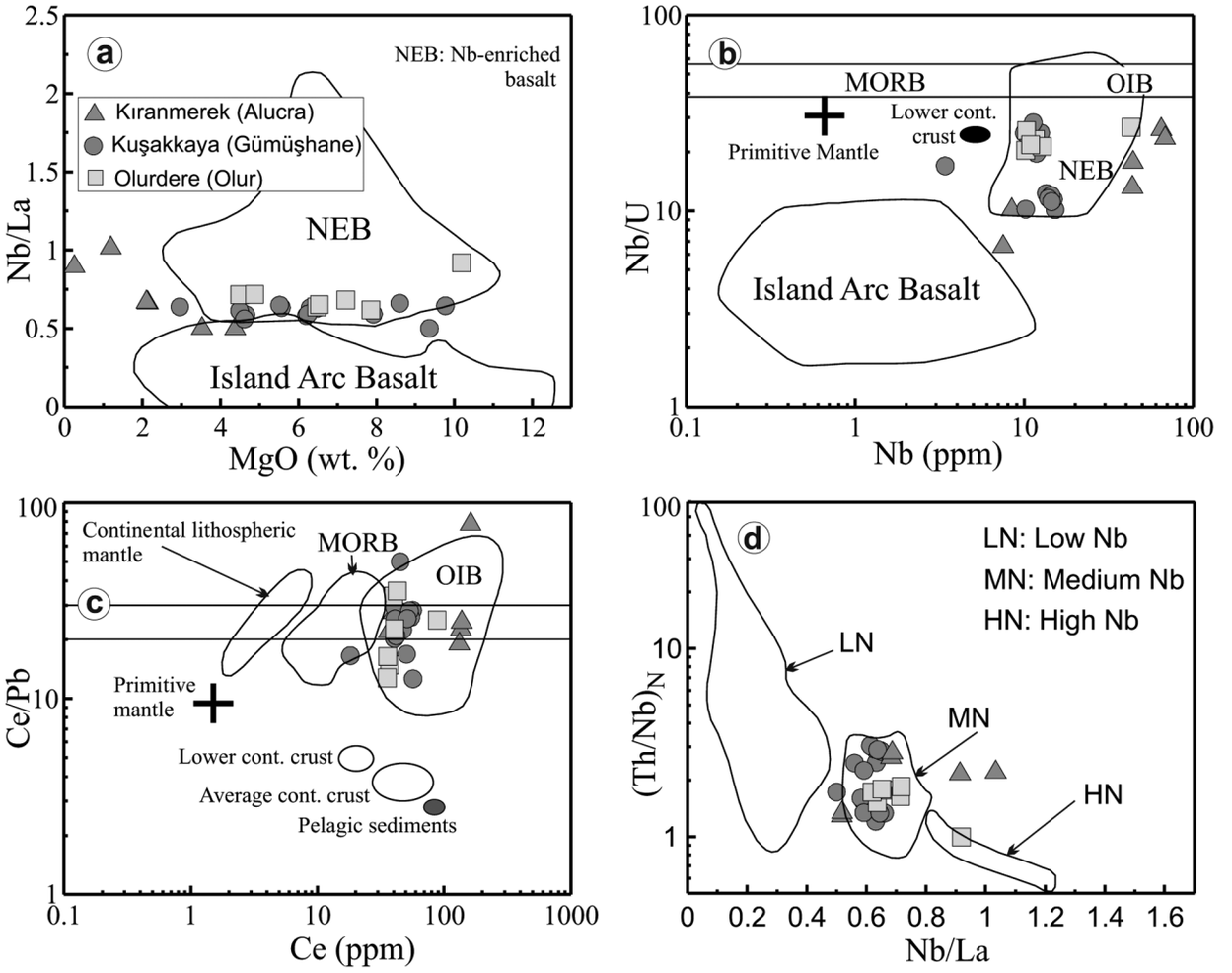

Figure 7. Nb/La versus MgO (wt%) diagram (*a*; after Kepezhinskas et al. 1996), Nb/U versus Nb (ppm) diagram (*b*; after Kepezhinskas et al. 1996), Ce/Pb versus Ce (ppm) diagram (*c*; Hofman et al. 1986), and $(Th/Nb)_N$ versus Nb/La diagram (*d*; after Xia et al. 2013) for the Upper Jurassic basalts from the Alucra, Gümüşhane, and Olur regions of Turkey. Mid-ocean ridge basalt (MORB) and ocean island basalt (OIB) fields are after Hofman (1986). References for primitive mantle, lower continental crust, and average continental crust are given in Sims and De Paolo (1997). NEB = Nb-enriched basalt; $(Th/Nb)_N$ = primitive mantle–normalized Th/Nb (after McDonough and Sun 1995). A color version of this figure is available online.

above inferences (fig. 9). However, moderate to high MgO contents and Mg numbers, along with crust-like geochemical features (e.g., negative Nb-Ta anomalies), support the role of crustal assimilation. Notably, Nb-Ta troughs are also typical of basalts derived from the mantle wedge at subduction zones, an indication of subduction-related metasomatism in the source (e.g., Green and Pearson 1987; Schmidt et al. 2004).

Several other geochemical tools, such as Nb/U, Ce/Pb, La/Nb, Ta/Yb, Ti/Yb, and K/P ratios, may be utilized to detect crustal assimilation by basaltic magmas. For instance, Hofmann et al. (1986) showed that mantle-derived melts, such as MORBs and OIBs, have an average Nb/U ratio of 47 ± 10 and an average Ce/Pb ratio of 25 ± 5 (fig. 7*b*, 7*c*). By contrast, Nb/U and Ce/Pb ratios are much lower in both crustal materials (Nb/U = ~15; Ce/Pb = ~4.5) and pelagic sediments (Nb/U = ~4.5; Ce/Pb = ~2.5; Taylor and McLennan 1985) as a consequence of the relative enrichment of Pb and U. Therefore, mantle-derived basalts contaminated by crustal material are likely to have ratios lower than 40 for Nb/U and 20 for Ce/Pb. The Upper Jurassic basalts of the Sakarya Zone have Nb/U ratios averaging ~18, with a range from 10 to 40. Such average ratios suggest little contamination by continental material. By contrast, Ce/Pb ratios in the

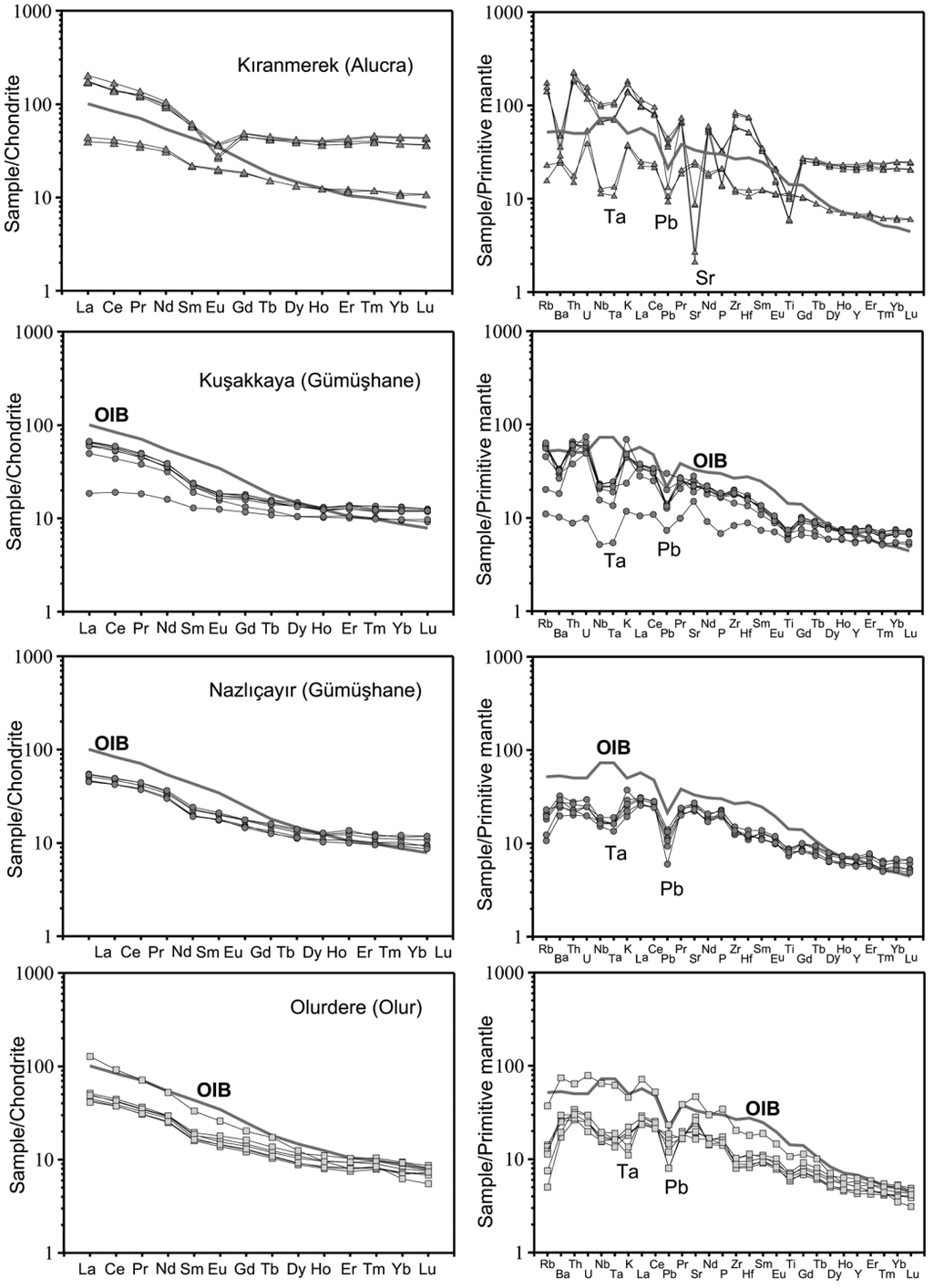

Figure 8. Chondrite-normalized rare earth elements and primitive mantle–normalized trace element patterns for the Upper Jurassic basalts. Data for ocean island basalts (OIBs) are from Sun and McDonough (1989). Chondrite and primitive mantle values for normalization are from Taylor and McLennan (1985) and McDonough and Sun (1995). A color version of this figure is available online.

Upper Jurassic basalts are 25 on average and range from 13 to 80, which are much higher than those of the continental crust and are close to and even higher than those of the MORBs and OIBs. This finding suggests that crustal contamination is not significant. Another striking feature of the Upper Jurassic basalts is that they have Nb and Ce contents as well as Nb/U and Ce/Pb ratios similar to

Table 2. Sr, Nd, and Pb Isotopic Compositions of the Upper Jurassic Basalts from the Alucra, Gümüşhane, and Olur Regions of Turkey

Sample	Rb (ppm)	Sr (ppm)	Sm (ppm)	Nd (ppm)	$^{87}Rb/^{86}Sr$	U (ppm)	Th (ppm)	Pb (ppm)	$^{87}Sr/^{86}Sr$	2s	I_{Sr}	$^{147}Sm/^{144}Nd$	$^{143}Nd/^{144}Nd$	2s	$\varepsilon_{Nd}(0)$	$f_{Sm/Nd}$	$\varepsilon_{Nd}(t)$	T_{DM} (Ga)	$^{206}Pb/^{204}Pb$ i	$^{207}Pb/^{204}Pb$ i	$^{208}Pb/^{204}Pb$ i
N-4	11	533	5.18	24.0	.06	.5	2.1	.9	.70446	8	.70433	.1311	.51273	7	1.9	−.33	3.2	.67	17.82	15.57	37.59
N-6	6	448	4.52	21.3	.04	.4	1.6	1.4	.70446	9	.70437	.1289	.51273	10	1.8	−.34	3.2	.67	18.27	15.60	38.23
N-8	14	460	4.44	21.3	.09	.5	1.7	2.0	.70445	13	.70426	.1266	.51275	9	2.1	−.36	3.5	.65	18.22	15.60	38.25
KS-1	37	492	5.50	27.1	.22	1.5	4.5	2.0	.70497	9	.70449	.1232	.51272	10	1.6	−.37	3.1	.69	17.60	15.58	37.74
KS-2	35	432	5.45	27.6	.23	1.3	5.2	2.1	.70473	9	.70422	.1199	.51270	9	1.2	−.39	2.7	.73	17.80	15.59	37.63
KS-5	27	558	4.38	22.4	.14	1.0	3.0	2.0	.70491	9	.70459	.1187	.51273	10	1.8	−.40	3.4	.67	17.97	15.60	38.10
U-3	7	299	2.99	11.4	.06	.2	.7	1.1	.70450	10	.70436	.1593	.51276	8	2.5	−.19	3.2	.62	18.29	15.60	38.34
OP-8	5	386	4.49	21.0	.03	.6	2.7	1.2	.70562	9	.70554	.1298	.51272	7	1.5	−.34	2.9	.70	18.00	15.58	37.87
OP-21	9	482	3.92	19.8	.05	.5	2.1	2.5	.70501	10	.70490	.1202	.51272	7	1.7	−.39	3.2	.68	18.29	15.59	38.28
OP-22	8	562	3.69	17.8	.04	.4	2.2	2.2	.70494	10	.70484	.1259	.51270	8	1.2	−.36	2.7	.72	18.31	15.58	38.19
OP-24	7	393	4.27	20.9	.05	.6	2.5	1.8	.70476	10	.70464	.1241	.51275	9	2.1	−.37	3.6	.65	18.20	15.58	38.21
OP-26	22	932	7.65	37.4	.07	1.9	6.8	3.5	.70463	9	.70448	.1242	.51272	10	1.6	−.37	3.1	.69	17.78	15.52	38.05
KM-1	85	172	13.82	71.4	1.43	2.4	14.4	5.8	.70688	9	.70372	.1175	.51278	9	2.7	−.40	4.2	.60	18.05	15.59	37.78
KM-4	14	463	4.99	22.0	.09	1.1	1.2	1.6	.70437	8	.70418	.1377	.51280	9	3.2	−.30	4.4	.56	17.71	15.56	38.24
KM-5	10	493	5.08	23.5	.06	.8	1.4	1.4	.70419	10	.70406	.1313	.51278	5	2.7	−.33	4.0	.60	17.86	15.57	38.15

Note. $\varepsilon_{Nd} = [(^{143}Nd/^{144}Nd)_s/(^{143}Nd/^{144}Nd)_{CHUR} - 1] \times 10{,}000$, $f_{Sm/Nd} = (^{147}Sm/^{144}Sm)_s/(^{147}Sm/^{144}Sm)_{CHUR} - 1$, $(^{143}Nd/^{144}Nd)_{CHUR} = 0.512638$, and $(^{147}Sm/^{144}Sm)_{CHUR} = 0.1967$. The model ages were calculated using a linear isotopic ratio growth equation: $T_{DM} = 1/l \times \ln(1 + [(^{143}Nd/^{144}Nd)_s - 0.51315]/[(^{147}Sm/^{144}Nd)_s - 0.2137])$. DM = depleted mantle; CHUR = chondritic uniform reservoir; i = initial.

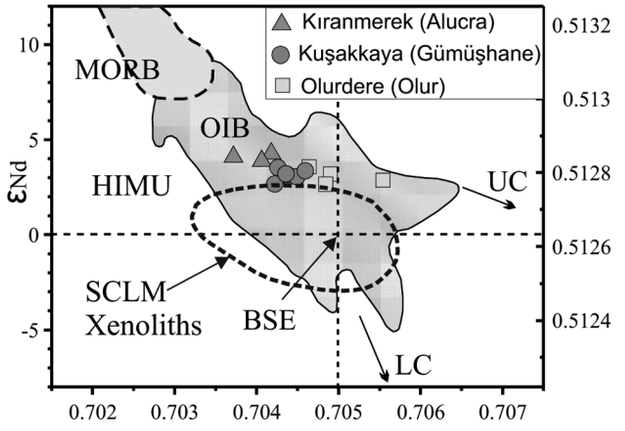

Figure 9. Initial ε_{Nd} versus I_{sr} diagram (after Zindler and Hart 1986) for the Upper Jurassic basalts. The field for subcontinental lithospheric mantle (SCLM) xenoliths is from Erlank et al. (1987), and mid-ocean ridge basalt (MORB) and ocean island basalt (OIB) fields are from Sun and McDonough (1989). BSE = bulk silicate earth; HIMU = high-μ mantle source; LC = lower crust; UC = upper crust. A color version of this figure is available online.

those of NEBs, as shown in the diagrams in figure 7, a feature of basalts derived from the metasomatized mantle wedge by asthenospheric melts.

Accordingly, incompatible/compatible element ratios, such as La/Nb, Th/Yb, and La/Ba, are also useful indicators of crustal contamination because La, Ba, and Th increase relative to Nb and Yb if basaltic magma is contaminated by continental material, which usually has high La/Nb, Ba/Nb, and Th/Yb ratios and a low La/Ba ratio (Weaver and Tarney 1984; Wedepohl 1995). The Upper Jurassic rocks plot just above the line of mantle array, implying that the parental melt has been contaminated by a certain Th-rich crustal material (fig. 11*a*). However, such Th enrichment may have been caused by sediment melt metasomatism of the mantle source. In the diagram of La/Nb versus La/Ba (fig. 11*b*), all the Upper Jurassic mafic rocks do not display a distribution along the arrow trending toward the lithosphere, a feature of mafic melts contaminated by crustal and/or subcontinental lithospheric components. Instead, the samples plot in the field of OIBs (Fitton et al. 1991). In conclusion, crustal contamination appears to be negligible for the Upper Jurassic basalts. Moderate negative Nb/Ta anomalies, although implying a certain degree of crustal contamination of the rocks, are believed to have been inherited from the mantle source. Low to moderate MgO contents and Mg numbers are caused by magmatic differentiation, which is discussed in more detail in the next subsection.

Fractional Crystallization. The Upper Jurassic basalts are characterized by high ranges of major elements (SiO_2 = 44.6–52.4 wt%; MgO = 3.5–10.2 wt%) and highly compatible trace elements (Ni = 15–171 ppm; Cr = 48–328 ppm) and Mg numbers (23–51), suggesting that primary magmas have undergone fractional crystallization. Strong negative Sr and Eu anomalies are detected in the evolved samples (dacites) of the Kıranmerek Member, arguing for a significant fractionation of plagioclase. Negative correlations of Ni and TiO_2 against SiO_2 (fig. 12*a*, 12*b*) and a positive correlation between MgO and total Fe_2O_3 (not shown) indicate that Fe-Mg-rich

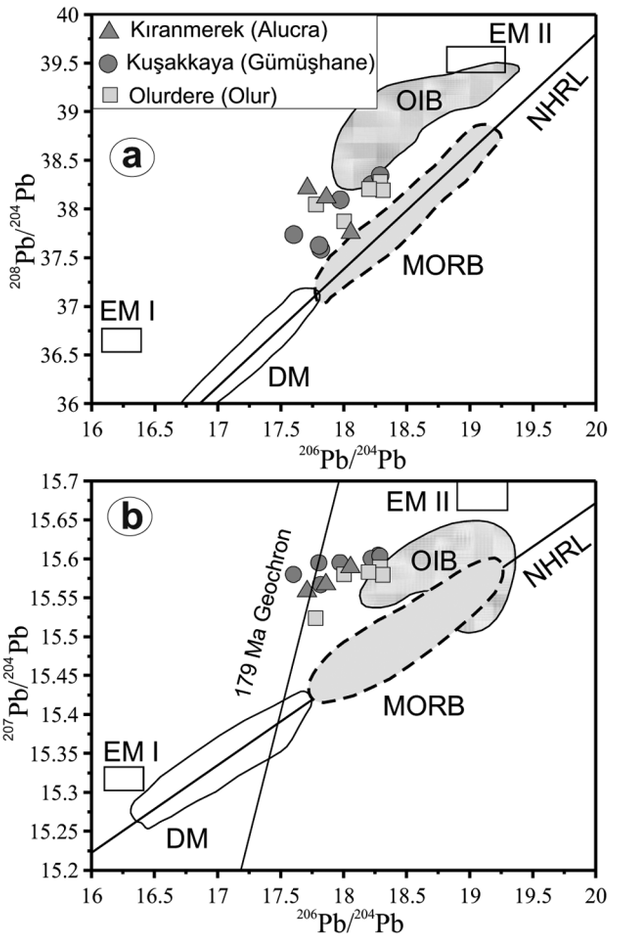

Figure 10. Initial $^{208}Pb/^{204}Pb$ versus $^{206}Pb/^{204}Pb$ (*a*) and $^{207}Pb/^{204}Pb$ versus $^{206}Pb/^{204}Pb$ (*b*) diagrams. Fields for enriched mantle (EM) I, EM II, mid-ocean ridge basalts (MORBs), ocean island basalts (OIBs), and the Northern Hemisphere reference line (NHRL) are from Zindler and Hart (1986). DM = depleted mantle source. A color version of this figure is available online.

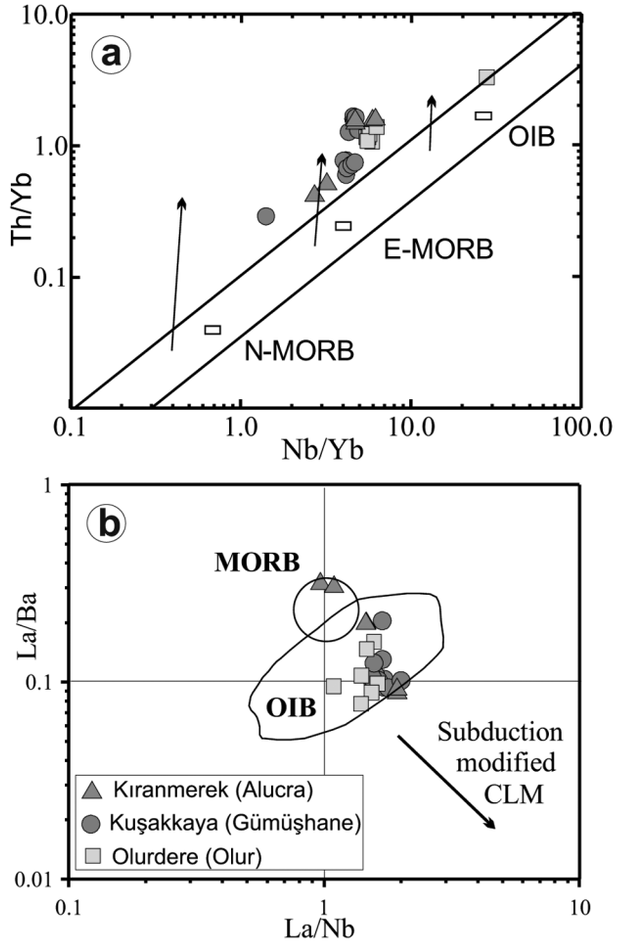

Figure 11. *a*, Th/Yb versus Nb/Yb plot for the Upper Jurassic basalts. Th/Yb ratios slightly higher than the mid-ocean ridge basalt (MORB)–ocean island basalt (OIB) array may represent little effects of crustal contamination. *b*, La/Ba versus La/Nb plot. Absence of dispersion to higher La/Nb and lower La/Ba ratios represents arguments against the effects of lithosphere contamination. The fields for OIB and MORB are from Saunders et al. (1992) and Sun (1980). A color version of this figure is available online.

phases, such as clinopyroxene and olivine, were fractionated after the lavas reached the surface. The presence of voluminous large clinopyroxene and small to moderate iddingsite (transformed after olivine) in the rocks also indicates that the basaltic magma has resided at hypabyssal depths for a period of time and undergone a certain degree of clinopyroxene (and olivine) fractionation before eruption to the surface. A similar approach can be put forward for the plagioclase because of its abundance in thin sections. However, its occurrence as small crystal laths, the lack of negative Eu anomaly, and the presence of slightly positive Sr anomaly indicate that plagioclase crystallized at a later stage.

However, the Mg numbers of the rocks lower than 40 seem inconsistent with the silica contents lower than 52 wt% and the mineralogical mode including clinopyroxene and olivine. Such a phenomenon is due to the relative enrichment in total Fe_2O_3 (8.8–14.0 wt%) during magmatic differentiation. As shown in the variation diagrams (fig. 12*c*, 12*d*), the rocks display trends of slightly increasing Fe_2O_3 and TiO_2 with decreasing Mg number, which are unexpected for a natural system evolving from basalt to silica-rich and iron-poor andesitic products (Bowen's reaction series; Bowen 1928). The variation trend of increasing Fe with decreasing Mg number in a magmatic system is known as the Fenner variation trend (Fenner 1929), and natural examples, although rather rare, are found in volcanic tholeiitic suites (e.g., Carmichael 1964), MORBs (e.g., Lehnert et al. 2000), late-stage ferrobasalts in gabbros (e.g., Natland and Dick 2001), layered intrusions (e.g., Duchesne et al. 2006), and flood basalts (e.g., Hooper 2000; Xu et al. 2003). As many authors have pointed out, magnetite fractionation in magmatic differentiation is mainly controlled by oxygen fugacity (fO_2; Osborn 1959; Veksler 2009). Si enrichment and Fe depletion in residual liquids are due to the increasing oxygen fugacity in response to the magnetite fractionation in the early stage of differentiation (Osborn 1959; Toplis and Carrol 1995). In the case of low fO_2, Fe is enriched for a long time in the residual liquid, as the onset of magnetite crystallization is delayed (Jang et al. 2001).

The field characteristics of the Upper Jurassic basalts of the eastern Sakarya Zone are similar to those of flood basalts. Petrographic observations show that magnetite is abundant but occurs in the form of small grains in thin sections, unlike clinopyroxene. When evaluated together with the negative variations in Mg numbers with total Fe_2O_3 and TiO_2, relatively low fO_2 can be suggested to have prevailed in the early stage of and even throughout differentiation, thereby leading a delay to some extent of the crystallization of magnetite and other Fe-Ti oxides. As a result, the residual liquid evolved to be more enriched in Fe instead of Mg, which is the opposite of what is expected for the fractional crystallization of basaltic melts, thereby resulting in the formation of unexpectedly low Mg numbers (23–35) in the rocks.

Nature of Mantle Source. A useful approach to understanding the nature of the source can be improved if magmas are free from the effects of crystal fractionation and crustal contamination. The com-

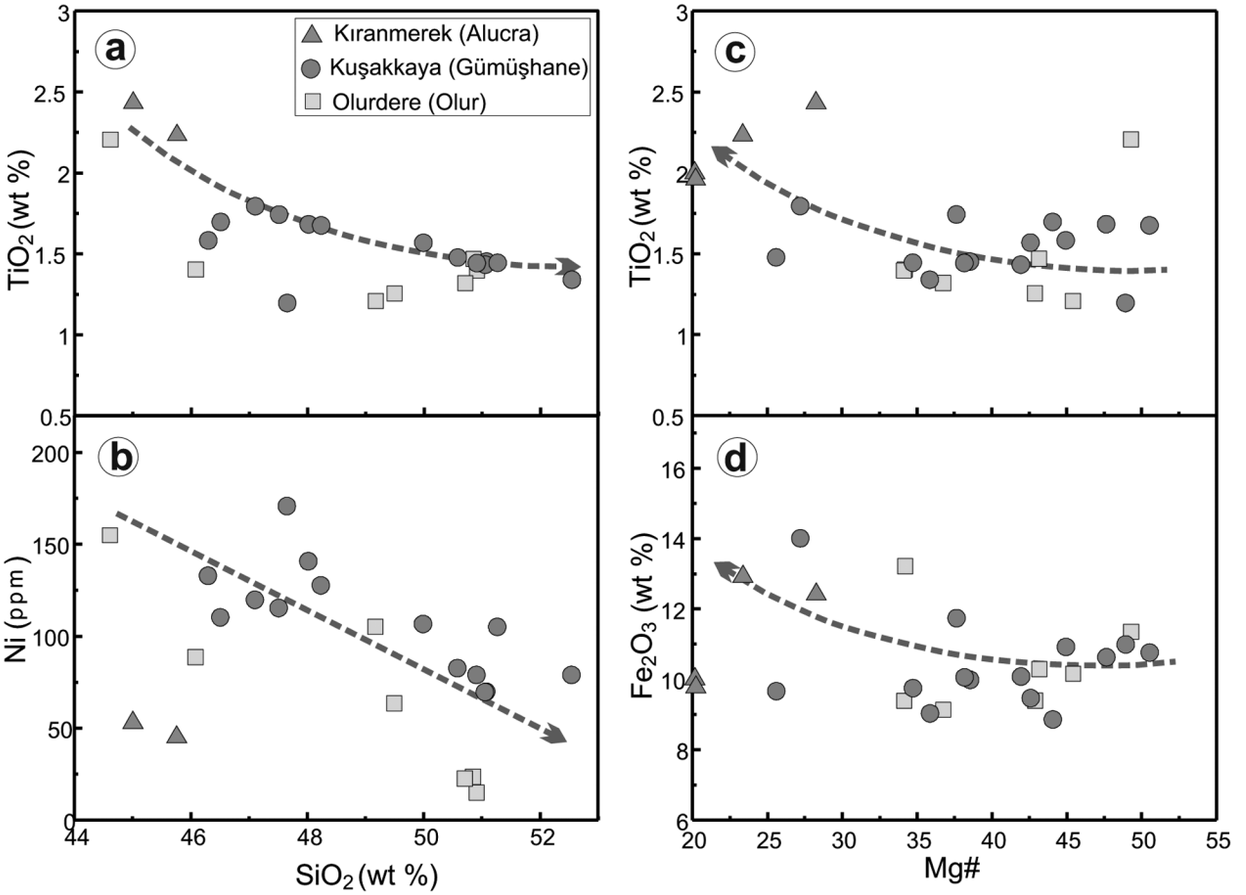

Figure 12. TiO_2 and Ni versus SiO_2 (*a*, *b*) and TiO^2 and Fe_2O_3 versus Mg number (*c*, *d*) variation diagrams. Mg# = MgO/(MgO + Fe_2O_3 × 0.889). A color version of this figure is available online.

positional range of such a primitive melt is a direct result of the compositional nature of the source plus the degree of melting. Some samples have MgO, Ni, and Cr concentrations higher than 6 wt%, 150 ppm, and 250 ppm, respectively. These approach those of primitive melts in equilibrium with mantle peridotites. Fractionation between light rare earth elements (LREEs) and HREEs, enrichment of LILEs, depletion of HFSEs, and slight to moderate negative Nb, Ta, and Ti anomalies are widely ascribed to the derivation from a refractory lithospheric mantle source. Unradiogenic $^{87}Sr/^{86}Sr$ ratios (0.70372–0.70418), moderately positive ε_{Nd} values (+2.7 to +4.4), and Pb isotope ratios plotted just above the NHRL are also consistent with a mantle source modified by continental materials and/or enriched mantle (EM) II–type mantle reservoir.

The Upper Jurassic basalts of the eastern Sakarya Zone are tightly clustered in the upper left quadrant of the Sr-Nd isotope diagram (fig. 9), essentially near the bulk silicate Earth composition, except for one sample that plots in the upper right quadrant. These values are consistent with those of the OIBs (Sun and McDonough 1989) and are also within the range of those of subcontinental lithospheric mantle xenoliths (Erlank et al. 1987), except for slightly higher ε_{Nd} values. The injection of crustal material into the mantle in subduction zones is one of the most widely accepted models to explain the formation of various mantle reservoirs from the depleted mantle. Pb isotopes are the most sensitive indicators of contamination of the mantle by crust-derived sediments because of the huge contrast in Pb abundances between sediments (19.9-ppm global subducting sediment; Plank and Langmuir 1998) and the mantle (0.150 ppm in PM; McDonough and Sun 1995). Upper crustal rocks and their sedimentary derivatives are characterized by $^{208}Pb/^{204}Pb$ and $^{207}Pb/^{204}Pb$ values that are considerably above those of the mantle array defined by data from oceanic basalts. An EM II–type mantle reservoir with elevated $^{208}Pb/^{204}Pb$ and $^{207}Pb/^{204}Pb$ ratios relative to those of the mantle array has affinities

with the upper continental crust. The Upper Jurassic basalts have initial $^{208}Pb/^{204}Pb$ and $^{207}Pb/^{204}Pb$ ratios that plot in a tight field already above the mantle array (fig. 10*a*, 10*b*), implying that the lithospheric mantle source was slightly metasomatized by the addition of slab melts possessing upper crust-like Pb isotopes. However, the Pb isotope ratios close to those of the OIBs, as shown in the diagrams (fig. 8), as well as OIB-like Sr and Nd ratios (fig. 7) argue against simple-source sediment contamination and may refer to the involvement of some melts from a deeper mantle source.

Relatively high K_2O contents and calc-alkaline nature coupled with the significant LILE enrichment suggest the involvement of volatile-bearing minerals such as phlogopite and amphibole, which are the major host phases for LILEs in a lithospheric mantle (Foley et al. 1996; Ionov et al. 1997; Yang et al. 2007). Melts originating from a phlogopite-bearing source may have a higher Rb/Sr ratio (>0.1) and a lower Ba/Rb ratio (<20), whereas melts in equilibrium with amphibole in their source are expected to have significantly high Ba and Ba/Rb ratio (>20) with a Rb/Sr ratio lower than 0.1 (Furman and Graham 1999). As shown in figure 13*a*, the samples from the Kuşakkaya and Kıranmerek Members have Rb/Sr ratios lower than 0.1 and Ba/Rb ratios lower than 20 in general, pointing to a melting history in a refractory lithospheric mantle without K-bearing phases. However,

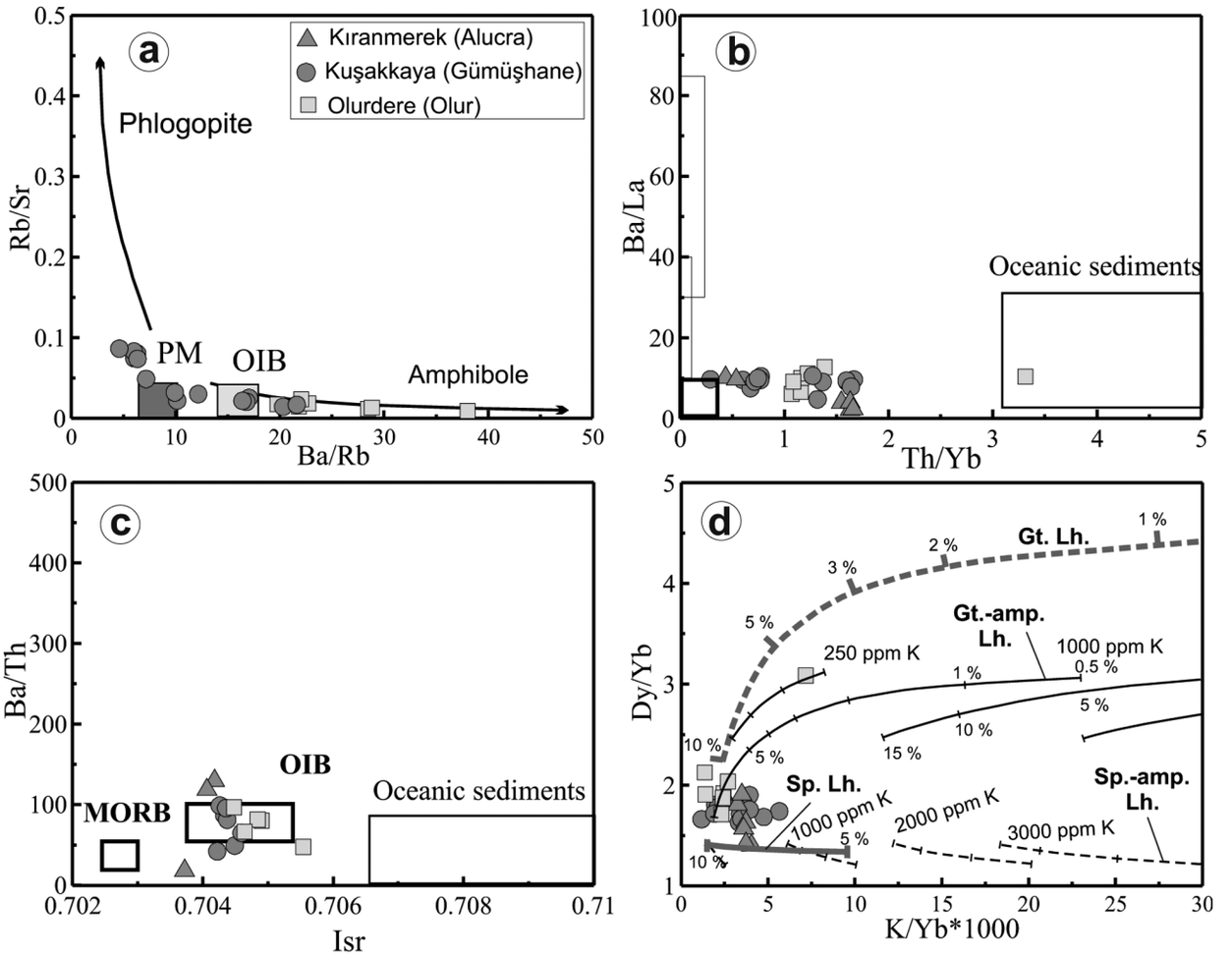

Figure 13. *a*, Rb/sr versus Ba/Rb plot for the basalts. *b*, *c*, Ba/La versus Th/Yb and Ba/Th versus I_{Sr} plots, implying the effects of oceanic sediments in the modification of mantle source. However, these elemental and isotopic ratios are consistent with those of the ocean island basalts (OIBs). *d*, Dy/Yb versus K/Yb × 1000 diagram for the Upper Jurassic basalts from eastern Sakarya Zone, Turkey. Melting curves for garnet lherzolite (Gt. Lh.), spinel lherzolite (Sp. Lh.), garnet-amphibole lherzolite (Gt.-amp. Lh.), and spinel-amphibole lherzolite (Sp.-amp. Lh.) are from Duggen et al. (2005). MORB = mid-ocean ridge basalt; PM = primitive mantle. A color version of this figure is available online.

the rocks from Olurdere display a Ba/Rb ratio higher than 20 and a Rb/Sr ratio lower than 0.1, implying the presence of amphibole rather than phlogopite as a K-bearing phase in the melting source.

The Upper Jurassic basalts show slight to moderate depletions of Nb-Ta, Zr-Hf, and Ti relative to neighboring elements in the PM-normalized patterns (fig. 8), all of which are attributed to the fluid-related metasomatism of a mantle source in a subduction zone (e.g., Elliot et al. 1997). However, when we compare these depletions of one group of basalts with those of the other groups, the degree of these depletions is decreased in basalts from Kıranmerek (Alucra) through Kuşakkaya (Gümüşhane) to Olurdere (Olur). Samples from the Nazlıçayır section of the Kuşakkaya and Olurdere display multielement patterns similar to those of the OIBs; in fact, one (OP-26) from Olurdere has a multielement pattern typical of OIBs (fig. 8). Furthermore, in contrast to the Lower Jurassic gabbros and basalts from the same region (Dokuz et al. 2006; Şen 2007; Genç et al. 2010), all the Upper Jurassic basalts interestingly demonstrate a moderate depletion in Pb, a feature inherited from a mantle source similar to that of normal OIBs (Edwards et al. 1994; Hofman et al. 1986; Zou et al. 2000; Ma et al. 2014). Accordingly, low enrichment of LREEs relative to HREEs (La_N/Yb_N = 1.9–6.3), except for OP-26 from Olurdere with a relatively elevated La_N/Yb_N (20.4), argue against generation from a strongly modified mantle by slab melts and even sediment melts, which would have elevated the LREE contents of the mantle source.

To test this hypothesis, we assessed our samples using Th/Yb versus Ba/La and I_{Sr} versus Ba/Th (fig. 13*b*, 13*c*, respectively), as these variables are reliable indicators of potential sediment or fluid contributions to magma source regions (Woodhead et al. 2001). The contribution of fluids or melts released from subducted marine sediments to the mantle source is represented in these diagrams by deviation to the right side toward high Th/Yb and I_{Sr}, whereas vertical increases in Ba/La and Ba/Th ratios are ascribed to the melt or fluid advection from the altered oceanic crust. The Upper Jurassic basalts plot just over and commonly on the right side of the MORB field, similar to the field of OIBs but not to the field of oceanic sediments. This case can be interpreted in three ways: (1) OIB-like element ratios and I_{Sr} values were inherited directly from the OIB-like sublithospheric mantle, (2) fingerprints of previous sediment melt and/or fluid contributions to the mantle reservoir may have been gradually diminished by subsequent partial-melting events, and (3) a mixture of melts from the MORB mantle and the OIB-like sublithospheric mantle occurred, as particularly implied by the distribution of Th/Yb ratios between the MORB and the OIB fields.

The K/Yb versus Dy/Yb diagram obtained by Duggen et al. (2005; fig. 13*d*), which shows geochemical modeling results for mantle-derived rocks, provides constraints on the composition of the mantle source and the degree of partial melting in the spinel stability field or the garnet stability field that produced the parental magmas of the Upper Jurassic basalts. The samples with MgO contents lower than 4 wt% are not plotted because of uncertainties arising from the fractionation of their major and trace element compositions. High Dy/Yb ratios (>2.5) are typical of partial melts produced in the garnet stability field, whereas partial melts in the spinel stability field have low Dy/Yb ratios (<1.5). All the samples except for one have Dy/Yb ratios ranging from 1.7 to 2.1, with an average value of 1.8. These values are lower than 2.5 and higher than 1.5 and therefore do not offer a clear indication of the presence of either garnet or spinel in the source. However, the samples cluster mostly at the end of the partial-melting curves (fig. 13*d*), modeled according to three different scenarios, that is, partial melting of (1) a garnet lherzolite source, (2) a garnet-facies amphibole lherzolite source, and (3) a spinel-garnet lherzolite source. This clustering suggests the involvement of garnet rather than spinel in the source. For a wide range of partial melting (1%–15%) from an amphibole-bearing spinel lherzolite source, K/Yb and Dy/Yb ratios remain above 5 and below 1.5, respectively. Therefore, melts from an amphibole-bearing (and phlogopite-bearing) spinel lherzolite source seem to be inadequate to produce low K/Yb and relatively high Dy/Yb ratios in the rocks. By contrast, nearly 10% melting of 1000-ppm K-bearing garnet-facies amphibole lherzolite source or spinel-garnet lherzolite source can explain the moderate K/Yb and Dy/Yb ratios of the Upper Jurassic basalts. Moreover, sample OP-26 from Olurdere has a relatively high Dy/Yb ratio (3.1), pointing to the existence of residual garnet alone or the coexistence of garnet and spinel in the lherzolite source, as garnet preferentially incorporates the HREEs. The other samples may represent the products of higher degrees of melting of such a garnet-facies amphibole lherzolite or a garnet-spinel lherzolite source. All these inferences refer to a deep partial-melting event, most probably in the spinel-garnet transition zone at depths of ~70–100 km (Duggen et al. 2005).

Despite all these inferences, melting in the spinel-transition zone alone seems insufficient to explain the hump-shaped PM-normalized patterns similar to those of the intraplate basalts and the OIBs; the decrease in the troughs of the Nb-Ta, Zr-Hf, and Ti anomalies, probably suggesting the weakening or

erasing of earlier traces of subduction components; and the negative Pb anomalies possibly inherited from a sublithospheric mantle. An interaction between a mantle plume material, such as OIB, and subcontinental mantle or melts therefore could provide an alternative explanation for the aforementioned points. This model can also explain LILE/HFSE and LREE/HFSE ratios lower than those in classical island arc basalts (Petrone et al. 2003) as well as Nb/La, Th/Nb, and Nb/U ratios similar to those in the NEBs (fig. 7), in which these element ratios are higher than those in the classical island arc basalts (Kepezhinskas et al. 1996). As a result, lithospheric mantle melting modified by subduction fluids alone appears to be incapable of producing these elemental and isotopic ranges in the Upper Jurassic basalts; thus, addition of an OIB-type component in the mantle source is most probably involved.

Tectonic Setting: Active Subduction versus Slab Breakoff. The evidence presented above for the petrogenesis of the Upper Jurassic mafic rocks coupled with the Lower Jurassic rocks can be used to test alternative plate tectonic models for the Jurassic period in the Sakarya Zone.

Except for very few Permian locations, no geological records documenting the Permian and Triassic events in the Sakarya Zone are available. Almost in all parts, the Lower Jurassic Şenköy Formation lies unconformably over a Carboniferous crystalline basement (fig. 2). Mafic volcanic rocks and volcaniclastic sedimentary rocks dominate the unit (Kandemir 2004; Dokuz and Tanyolu 2006; Akdoğan et al. 2012). The formation exhibits highly variable thickness over a very short distance as well as upward decreases in grain size and bed thickness (Kandemir 2004), which are the main sedimentologic feature of formations accumulated in the basins in the early transgressive period.

Two geodynamic models have been proposed for the Late Triassic to Early Jurassic evolution of the Sakarya Zone, both of which are based on the aforementioned stratigraphic and sedimentologic characteristics of the Şenköy Formation. Some authors (Şengör and Yılmaz 1981; Görür et al. 1983; Yılmaz et al. 1997) have considered the Şenköy Formation as a backarc basin deposit, indicating the opening of the Neotethys Ocean behind Cimmeria (Sakarya Zone), a continental fragment that rifted from the northern margin of Gondwana and drifted northward during the Late Triassic to Early Jurassic. Other authors (Adamia et al. 1977; Golonka 2004; Okay et al. 2014) have also proposed an accumulation within a rift basin for Lower Jurassic sediments. However, unlike the previous group of authors, they have suggested that this basin was opened along the southern margin of Laurasia—particularly on the accretionary complex, not behind a continental fragment—during the northward subduction of the Tethys Ocean.

In the 2000s, geochemical data began to be widely used to understand Jurassic tectonic events. However, these efforts seem insufficient to reach a consensus because each group of authors has interpreted and exploited geochemical data to strengthen their tectonic views. Comments based on geochemical data appear to be correct from both tectonic views only because the region is placed in the backarc setting in the southward subduction model and in the forearc setting in the northward subduction model. Considering the spatial proximity to the arc, the subduction-related features can easily be obtained for the rocks from both forearc and backarc settings (Dokuz et al. 2006; Şen 2007; Genç and Tüysüz 2010; Karslı et al. 2014; Okay et al. 2014). Nevertheless, instead of the subduction signature of the Lower Jurassic igneous rocks, their compositional nature may be the more important consideration. Almost all of the Lower Jurassic igneous rocks have basaltic composition. Thus, a backarc—or at least an arc under the effect of an extensional regime—is required for the swift upwelling of mantle-derived mafic magma to Earth's surface without contamination by crustal rocks and differentiation to more felsic derivatives.

After a time gap of ~15–20 m.yr., magmatism was repeated in the Late Jurassic throughout the Sakarya Zone (fig. 2; Nzegge et al. 2006; Dokuz et al. 2010; Evcimen et al. 2014; this study). We believe that compared with the geochemical signatures of the Lower Jurassic rocks, the geochemical signatures of the Upper Jurassic rocks combined with the structural, stratigraphic, and sedimentologic data given in the earlier articles can supply a more precise constraint on the geodynamic evolution of the Sakarya Zone. Our view is that a slab-breakoff mechanism subsequent to a continental arc–continent collision explains the generation of Late Jurassic magmatism in the Sakarya Zone. The reasons for our model are backed by the following: (1) inferences from geochemical data, (2) the time gap between the two Jurassic magmatisms, (3) the spatial pattern of the rocks, (4) the stratigraphic and sedimentologic features of the Upper Jurassic rocks, and (5) epirogenic-type versus orogenic-type deformations. The reasons for these are discussed in more detail in the following subsections.

Inferences from Geochemical Data. Collisional magmatism does not have unique geochemical features. These rocks can have geochemical characteristics identical to those from active subduction and to those from intraplate settings, such as OIBs and

within-plate rocks (e.g., Roberts and Clemens 1993; Barbarin 1999). However, the rocks having subduction signatures are typically much more voluminous. Therefore, distinguishing subduction-related from collision-related magmatism is difficult with the use of geochemical data only. From the chondrite-normalized plot (fig. 8), a slightly negative REE profile with negative or positive Eu anomaly is one of the characteristics of rocks generated in subduction zones. LILE enrichment relative to HFSEs; prominent negative Nb-Ta, Zr-HF, and Ti anomalies; and prominent positive Pb anomaly in the PM-normalized diagrams (fig. 8) are the other features employed for the identification of subduction components in the rocks. However, all these features are also signatures of most rocks from collisional settings. One of the issues that needs to be considered is that the geochemical signatures of magmas depend not only on the prevailing *PT* conditions during partial melting but also on the protolith composition.

During collisional events, the crustal rocks located at the plate boundary, which were also formed previously by subduction processes, can be melted by slab breakoff and/or delamination. Consequently, the daughter melts derived from these rocks will have subduction signatures, as these signatures can be inherited from the precursor. This mechanism is also valid for the mafic rocks derived from a lithospheric mantle previously metasomatized by subduction fluids. Thus, subduction or arc fields in tectonic discrimination diagrams may not always refer to active subduction. Therefore, caution is needed when drawing conclusions from tectonic discrimination diagrams. For example, the occurrence of some rocks with collisional characteristics, even though they exist together with rocks with subduction signatures, is a strong indication of a collisional setting rather than active subduction because for a rock to have a collisional signature during active subduction is almost impossible. By contrast, owing to the aforementioned reasons, finding rocks possessing subduction signatures is possible in a collisional setting.

With their geochemical affinities varying from subduction to intraplate (figs. 7, 8), the Upper Jurassic magmatic rocks of the Sakarya Zone constitute a good example of this case. One group of authors (Ustaömer and Robertson 2010; Ustaömer et al. 2013; Okay et al. 2014) has suggested that the arc-like signature of these rocks and their regional metamorphism are due to the northward subduction of the Tethys Ocean beneath the Sakarya Zone. In this model, advective heat transfer from the injected mafic magmas is considered sufficient for the source of heat needed for the high-temperature metamorphism in midcrustal levels.

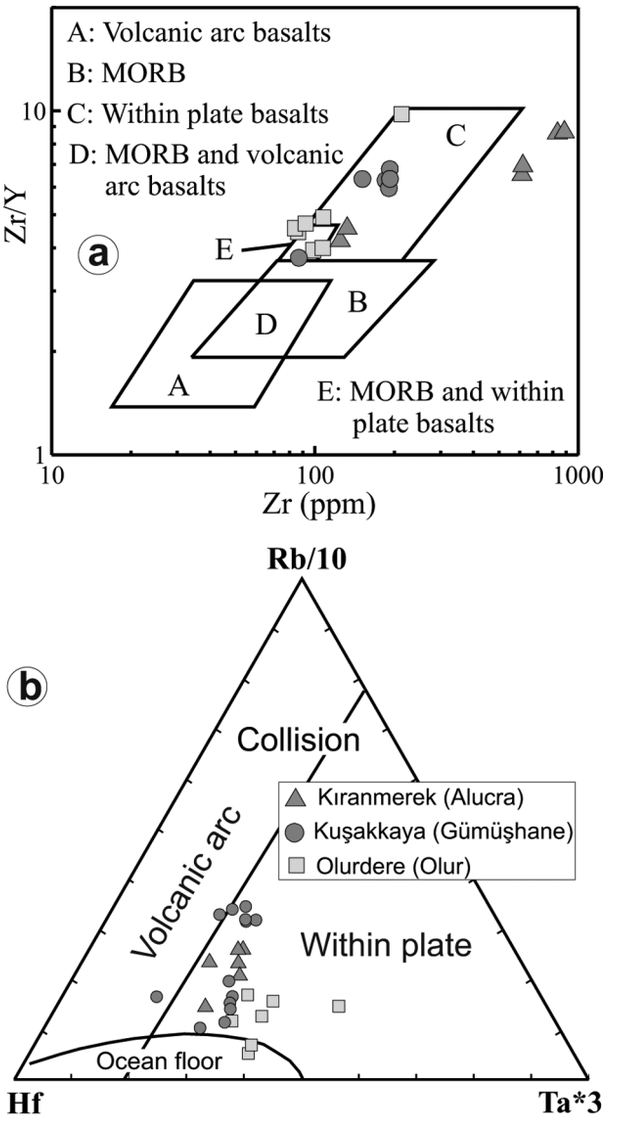

Figure 14. Tectonic setting of the Upper Jurassic basalts from the eastern Sakarya Zone. *a*, Zr/Y versus Zr (ppm) suitable for noncumulate basalts (after Pearce and Norry 1979). *b*, Rb/10-Hf-Ta*3 ternary plot for different tectonic settings (after Harris et al. 1986). MORB = mid-ocean ridge basalt. A color version of this figure is available online.

Collision signatures were first documented by Dokuz et al. (2010) in the Upper Jurassic shallow-level granitic intrusions from the Yusufeli area. Basaltic rocks in this study have stronger geochemical characteristics for generation in a collisional setting. They display Nb (44–76 ppm) and Ta (2.6–4.2 ppm) values and Nb/U, Nb/La, and Ce/Pb ratios that are greater than those of island arc basalts, as shown in the diagrams (fig. 7). These values and ratios are consistent with those of NEBs and, at the

same time, those of OIB-like rocks (Hofman et al. 1986). Accordingly, Th/Yb, Nb/Yb, La/Ba, La/Nb, Ba/La, and Ba/Th ratios are in between MORBs and OIBs, and most of them overlap with OIBs. A similar case is shown in their Pb isotope ratios (fig. 10*a*, 10*b*), whereas Sr and Nd isotope ratios are consistent with those of the OIBs (fig. 9). Furthermore, rocks especially from the Nazlıçayır section and Olurdere show REE and multielement patterns approaching the hump shape similar to OIBs and within-plate basalts, whereas rocks from the Kuşakkaya section and Kıranmerek present mixed patterns between OIBs and basalt from the depleted mantle (fig. 8). In brief, these values are intermediate between those derived from lithospheric and asthenospheric mantle sources, indicating a magma source transition from lithospheric to asthenospheric mantle. Tectonic discrimination diagrams also offer consistent results inferred from the earlier figures for Upper Jurassic basalts. According to figure 14*a*, almost all the samples plot within the plate tectonic setting (Pearce and Norry 1979) except for four differentiated samples from Kıranmerek. On the triangular diagram of Rb/10-Hf-Ta*3 (fig. 14*b*), our samples fall in the field of within plate (Harris et al. 1986), which is consistent with the results shown in figure 14*a*.

The occurrence of the aforementioned OIB-like geochemical signals of the Upper Jurassic rocks seems to be impossible during an active subduction with moderate angles because during such a subduction the oceanic lithosphere constitutes a relatively colder inclined wall that impedes the upwelling of the asthenosphere-lithosphere boundary and, consequently, melting in the asthenospheric source. On the other hand, the slab breakoff, which we believe to be the geodynamic mechanism responsible for the Late Jurassic magmatism and associated regional metamorphism, presents environmental conditions suitable for producing melts parental to the Upper Jurassic magmatic rocks. In this mechanism, as the ruptured oceanic slab sinks away, the hot asthenosphere upwells to fill the gap (Davies and von Blackenburg 1995). Possible advection of fluids from the asthenosphere may modify the isotopic and chemical composition of the overriding lithosphere (fig. 15*c*). This upwelling also leads to heating of the overriding lithosphere, which is previously metasomatized by asthenospheric and subduction agents. Melting of such a metasomatized mantle can explain the chemical and isotopic signatures of the Upper Jurassic basaltic rocks, which show a decrease in the troughs of Nb, Ta, and Ti anomalies; negative Pb anomalies; LILE/HFSE ratios lower than those of the classical island arc basalt; and Sr, Nd, and Pb isotope ratios between MORBs and OIBs but closer to those of OIBs. Underplating of the basaltic magmatism, together with the heat conduction from the asthenosphere and decompression because of erosion from the uplifted roof, may induce crustal melting. The result is the generation of silicic magmatism. A mixture of mantle- and crustal-derived melts will produce hybrid rocks. The

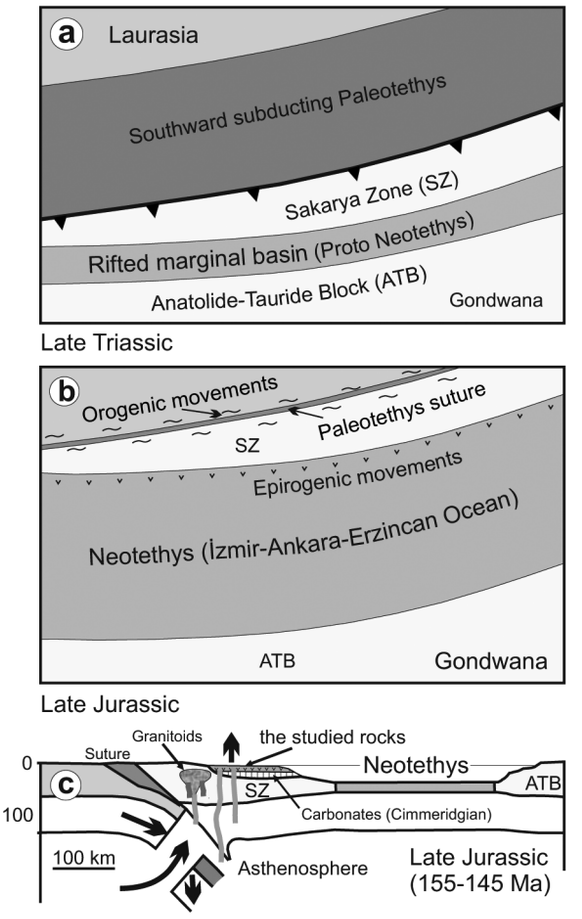

Figure 15. Tectonic model for the Upper Jurassic basalts discussed in this article. *a*, Northern branch of the Neotethys (İzmir-Ankara-Erzincan Ocean) as a backarc basin rifted from the northern margin of the Anatolide-Tauride Block (Gondwana) above a southward subduction zone (Şengör et al. 1984). *b*, Middle Jurassic welding of the Sakarya Zone (western terminal of Cimmeria) to Laurasia in the north caused a fold-and-thrust belt (orogenic movements) along this line, whereas epirogenic movements occurred in the south along the northern shelf of the Neotethys. *c*, Schematic cross section of the Sakarya Zone to the Anatolite-Tauride Block during the Late Jurassic. Breakoff of the Paleotethyan oceanic slab led to the generation of the parental melt of the Upper Jurassic basalts and epirogenic upwelling in the southern side of the Sakarya Zone (see text for details). A color version of this figure is available online.

geometric forms, spatial patterns, geochemical characteristics, and compositional range of the Upper Jurassic magmatic rocks are consistent with those generated by the processes of slab breakoff.

Time Gap between Two Jurassic Magmatisms. In the literature (Yılmaz and Boztuğ 1986; Okay and Şahintürk 1997; Saintot et al. 2006; Ustaömer and Robertson 2010; Adamia et al. 2011; Nikishin et al. 2012; Okay et al. 2014), the Sakarya Zone has been defined as a paleomagmatic arc from the Carboniferous through the Eocene. Northward subduction of a southerly situated Tethys Oceanic crust beneath Laurasia has been proposed by these authors for the Late Paleozoic to Mesozoic magmatic evolution of the Pontides, Caucasus, and Crimea. However, one of the outstanding signatures of this arc is that magmatism has occurred intermittently, for example, in the Late Carboniferous, Early Jurassic, Late Jurassic, Late Cretaceous, and Early-Middle Eocene. Periods of magmatic silence are much longer than the periods of magmatic activity. After a long intermittence subsequent to the Late Carboniferous igneous activity, the time span from 200 to 175 Ma (Early Jurassic) recorded a second major phase of magmatic activity (Şengör et al. 1993; Dokuz et al. 2006; Genç and Tüysüz 2010; Meijers et al. 2010; Okay et al. 2014). Except for one or two basic/intermediate intrusives and felsic extrusives, this magmatic phase is characterized by pillow lavas and, to a lesser extent, by basaltic pyroclastic rocks and diabase dikes. Other igneous activity in the Jurassic era is intensified between 155 and 145 Ma (Early Kimmeridgian–Late Tithonian), corresponding to the early stages of carbonate deposition in the Neotethys Ocean (Nzegge et al. 2006; Dokuz et al. 2010; Evcimen et al. 2014; this study). However, throughout an ongoing subduction, we cannot see any reason to switch to such a magmatic silence after basic volcanism, particularly in such an extensional arc. We therefore suggest that the above-mentioned time pattern of the Late Jurassic magmatism is more consistent with a slab breakoff.

Spatial Pattern of the Rocks. Recent investigations show that the Jurassic magmatism in the Sakarya Zone is temporally intensified in two stages: (1) the Early Jurassic and (2) the Late Jurassic. Both the Early and the Late Jurassic magmatisms are mainly recorded in the Şenköy Formation (Kandemir and Yılmaz 2009), which is widespread particularly in the southern part of the Sakarya Zone and constitutes the lateral equivalent of the Sada Formation (Okay et al. 2014) and the Mudurnu Formation (Tüysüz and Genç 2010) in the western and central Sakarya Zone. In its outcrops farther west, the unit is totally devoid of volcanism.

The Late Jurassic magmatism was first reported by Yılmaz and Boztuğ (1986) from the Kastamonu area in the central part of the Sakarya Zone (Nzegge et al. 2006; Okay et al. 2014). Recent studies, including the present study, reveal the presence of a widespread Late Jurassic magmatism in the eastern part of the Sakarya Zone (Dokuz et al. 2010; Evcimen et al. 2014). In contrast to the Lower Jurassic magmatic rocks, which are commonly pillow lavas (Şen 2007), the Upper Jurassic ones typically occur in the form of intrusive bodies or stocks mostly less than 10 km^2 (Dokuz et al. 2010), except for a few flood-like pillow basalts that are the subject of this article. These intrusives are confined to a long linear/arcuate zone aligned in an east-west direction, especially along the southern flank of the arc. Another distinguishing feature of the Upper Jurassic rocks is that the intrusives are characterized by a large compositional spectrum, for example, from diorite to granite (Dokuz et al. 2010; Ustaömer et al. 2013; Evcimen et al. 2014). In brief, short-lived magmatic activity, large compositional spectrum, small sizes of intrusive/extrusive outcrops, and their linear distribution match well with the slab breakoff mechanism, which predicts small volumes of melt and a narrow linear zone of magmatism (Davies and von Blackenburg 1995).

Stratigraphic and Sedimentologic Features of the Upper Jurassic Rocks. The Upper Jurassic magmatic rocks are limited in volume compared with the Lower Jurassic ones. Except for the rocks of this study, there are a few small intrusive bodies (Dokuz et al. 2010; Ustaömer et al. 2013). Nevertheless, in the Lesser Caucasus (Armenia), the eastward continuation of the Sakarya Zone, Late Jurassic magmatic rocks are common (e.g., Mederer et al. 2013). Similarly, such rocks are also widely documented in the central Sakarya Zone to the west (Nzegge et al. 2006) and in the Crimea, Ukraine (Meijers et al. 2010). Might Late Jurassic magmatic rocks be more common in the eastern Sakarya Zone? Our suggestion is that the Late Jurassic magmatic rocks are much more abundant than those known to date, but there are some difficulties in the discrimination of Early and Late Jurassic magmatic rocks in the field. These difficulties can be summarized into two subgroups: (1) the nature and timing of the Late Jurassic magmatism and (2) the similarities between the Lower and Upper Jurassic sedimentary rocks.

One of the most prominent causes of failure is the difficulty in distinguishing Late Jurassic magmatism from earlier magmatism in this area. Magmatic rocks intrusive into the Variscan crystalline basement have been regarded as Carboniferous in age. The Çamlıkaya granitoid complex in the eastern

part of the Sakarya Zone can be given as an example of this situation (Ustaömer et al. 2013; Evcimen et al. 2014; A. Dokuz, unpublished data). This is also the case for the extrusive member of the Late Jurassic magmatism. As indicated by this study, it is represented by basaltic rocks similar to those of the Early Jurassic magmatism. Direct isotopic dating of these units has been difficult (Cüneyt Şen, Karadeniz Technical University, personal communication).

The second reason for the failure to identify Late Jurassic magmatism is the similarities between the Lower and Upper Jurassic sedimentary rocks. In the distal portion of the basin, carbonate deposition with a thickness up to 180 m was followed by accumulation of ~250-m-thick coarse clastic sediments (Dokuz 2000). By this, these carbonates form a pronounced horizon traceable over long distances, enabling the separation of the Upper Jurassic clastic sediments from those of the Early Jurassic in the field. Such a separation is not possible for the clastic sediments deposited in the proximal portion of the basin, which corresponds geographically to the more northern parts of the study areas. In these portions, the Upper Jurassic sediments directly overlie the heterogeneous Variscan basement and/or the Lower Jurassic rocks. This is also the case for the Late Jurassic basic volcanism. Therefore, almost all the Upper Jurassic mafic rocks in this stratigraphic position, which are more common, have been accepted as Early Jurassic.

This sharp transition from carbonate sedimentation into coarse clastic sedimentation for a short period is ascribed to the slab breakoff–related regional uplift. Then carbonate sedimentation dominated again in the basin throughout the Early Cretaceous (Pelin 1977), which is difficult without any clastic input in a foreland basin over a subduction zone. By contrast, such depositions seem to be possible on the passive margin of a marginal basin. Subsequent to the welding processes, a transition from a tectonically active to inactive period has been supplied in the northern shelf of the Neotethys, which was needed for the carbonate deposition throughout the Late Jurassic–Early Cretaceous. The time interval corresponding to the deposition of the first carbonate level, which separates the Lower and Upper Jurassic clastic rocks from each other, is thought to be short (15–20 m.yr.) but is enough for the down-going oceanic slab to break off from the bouyant continental lithosphere.

Epirogenic-Type versus Orogenic-Type Deformations. The generation of local disconformities in the region (fig. 4*c*, 4*d*) involve vertical movements. Such vertical movements of a continent are identified as epirogeny and are distinguished from orogeny by the absence of coeval shortening structures in the same area. The causes of epirogeny are not well known.

The Late Jurassic disconformities are close to ophiolite vestiges of the İzmir-Ankara-Erzincan suture (fig. 1*a*) that lies ~50 km to the south. According to the northward-subduction model (Golonka 2004; Robertson et al. 2004; Okay et al. 2006, 2014; Ustaömer and Robertson 2010), this suture represents one of the branches of the Tethys Ocean (Paleotethys) that closed in the Early Cenozoic. Alternatively, the southward-subduction model (fig. 15*a*) suggests the welding of the Sakarya Zone (Cimmeria) to the southern margin of Laurasia in the Middle Jurassic and the opening of the Neotethys as a backarc basin in the south of the Sakarya Zone (Şengör and Yılmaz 1981; Şengör et al. 1984; Yılmaz et al. 1997). In this case, the areas studied would have been in a backarc setting, perhaps at least 200 km from the line of collision. Slab breakoff after collision is an expected phenomenon. Our model requires that slab breakoff occurred as much as 10–15 m.yr. after collision (fig. 15*b*, 15*c*; van Hunen and Allen 2011). This event, in combination with upwelling asthenosphere, leads to rapid isostatic uplift since the dynamic subsidence caused by subduction is stopped and the orogen loses its large load resulting from the oceanic slab (e.g., Davies and von Blackenburg 1995). This type of uplift in the Late Jurassic in the northern shelf of the Neotethys could explain the rising of submerged topographic highs vertically above sea level prior to deposition of clastic sediments and the role of these highs as sites of temporary erosion. Topographic lows are still the sites of uninterrupted marine sedimentation. Transformation of the upwelling asthenosphere into mantle lithosphere based on cooling might cause these eroded highs to again subside below sea level. The beginning of clastic sedimentation at these sites resulted in the formation of local disconformities. In brief, slab breakoff seems to be the main cause of this short-lived epirogenic movement in the Late Jurassic backarc basin, which resulted in the formation of disconformities in the region.

Geodynamic Model

In the northward-subduction model, overall the Late Jurassic or Cimmerian events—that is, magmatism, regional metamorphism, and structural deformations—are associated with the welding of small continental terrains to the southern margin of Laurasia or to subduction-accretion processes (Ustaömer and Robertson 2010; Topuz et al. 2013;

Okay et al. 2014; Okay and Nikishin 2015). However, a mechanism for the exhumation of these metamorphics, which are unconformably covered by the Lower Cretaceous turbidites, has not been presented.

In the preferred model, the Paleotethys Ocean was to the north of the Sakarya Zone, which, at that time, constituted a part of the northern margin of Gondwana (fig. 15). Southward subduction of the Paleotethys beneath Gondwana from the Permian to the Middle Jurassic resulted in the opening of a series of marginal basins at different times in front of Gondwana. This subduction caused the Karakaya backarc basin in the Sakarya Zone in the Early Triassic to open (Şengör and Yılmaz 1981). This short-lived basin closed at the end of the Triassic (Şengör et al. 1984). Backarc extension in the Late Triassic is suggested to have caused the breaking up of the Sakarya Zone from the northern margin of Gondwana and its drift to the north because of the ongoing southward subduction. The result was the opening of the Neotethys (fig. 15*a*; Şengör and Yılmaz 1981; Görür et al. 1983; Yılmaz et al. 1997; Dokuz and Tanyolu 2006). The Şenköy Formation was deposited in the Early Jurassic during this rifting period (Kandemir 2004; Kandemir and Yılmaz 2009). The closing processes of Paleotethys ended in the Middle Jurassic by the soft collision of the Sakarya Zone with the southern margin of Laurasia (Şengör and Yılmaz 1981; Şengör et al. 1984; Yılmaz et al. 1997; Dokuz et al. 2010). The Paleotethys suture would then be located along the northern border of the Sakarya Zone (fig. 15*b*, 15*c*). The ophiolites that could be the remnants of the Paleotethys have not yet been identified in the areas farther east than Tokat. The easterly extension of the Paleotethys remnants could be exposed along the Great Caucasus and Transcaucasus ranges because there is a continuous deposition from the Devonian to the Late Jurassic (Dizi series). In addition, the absence of Variscan and Early Cimmerian (Triassic) deformations in the Dizi series (Adamia et al. 2011) is consistent with our predictions regarding the Paleotethys.

By the Middle Jurassic collision, the Neotethys to the south of the Sakarya Zone reached its maximum dimensions, and a transition from a tectonically active period to a more quiescent one characterized the northern shelf of the Neotethys basin. After nearly 15–20 m.yr. of carbonate deposition over the Şenköy Formation, the Paleotethys oceanic slab broke off from the following continental portion, which was also thinned and partly subducted (fig. 15*c*). This phenomenon led to a short-lived period of instability in the basin and the source areas. This period was recorded by the deposition of coarse clastic sediments either directly over the carbonates or after a local disconformity (see figs. 3*c*, 4*c*, 4*d*) occurred in deeper parts of the basin. In the coastal portion of the Neotethys, these clastic sediments were deposited over either Paleozoic basement rocks or the Şenköy Formation. Slab breakoff also led to the opening of a window for ascension of asthenospheric components to metasomatize the lithospheric mantle. Partial melting of the metasomatized mantle yielded the melts parental to the basaltic rocks of this study. Advection of heat from the asthenosphere and mafic magmatic underplating led to the melting of crustal materials. Silicic melts later intruded the crust and rose to Earth's surface to form their extrusive equivalents. This event provided a short break in the carbonate deposition in the northern passive margin of the Neotethys. Subsequent to this short-lived tectonic and magmatic activity, carbonate deposition continued until ~95–90 Ma.

Conclusions

Recent studies reveal the occurrence of Upper Jurassic magmatic rocks in the eastern part of the Sakarya Zone, although outcropping areas are not large. These areas crop out in small extrusive and intrusive bodies and are represented by calc-alkaline rocks. Basaltic flows of ~10–30 m thick occur within the Upper Jurassic sedimentary rocks in the Alucra, Gümüşhane, and Olur areas.

These Late Jurassic rocks have moderate Dy/Yb ratios with an average value of 1.8, implying partial melting in the spinel-garnet transition zone at depths around 70–100 km. Other geochemical signatures are consistent with derivation from a mantle modified by subduction-related fluids. An OIB-type component from the sublithospheric mantle appears to be capable of producing the observed elemental and isotopic composition of Upper Jurassic basalts.

Late Jurassic magmatic rocks are exposed in areas mostly less than 10 km^2 and display a wide lithological range, that is, from gabbro to granite in intrusives and basalt to rhyolite in extrusives. These rocks form a west-to-east-trending curvilinear zone. Geochemical characteristics, timing, and duration of the Late Jurassic magmatism as well as rock diversity and their spatial pattern are consistent with slab breakoff, which predicts a short duration of magmatism after a short time gap from that of active subduction, small volumes of melt, and a narrow linear zone of magmatism.

The Upper Jurassic clastic sediments were deposited either directly over a carbonate succession up to

180 m thick or above a disconformity. Such short-term clastic sediment deposition can be caused by slab breakoff, as it would cause short-term epirogenic movements.

The preferred tectonic model involves the Paleotethys Ocean in the north of the Sakarya Zone. Southward subduction of the Paleotethys beneath the Sakarya Zone at least from the Late Triassic to the Middle Jurassic resulted in the opening of the Neotethys as a marginal basin to the south of the Sakarya Zone, which was located at the northern margin of Gondwana. With the welding of the Sakarya Zone to the southern margin of Laurasia in the Middle Jurassic, a transition in sedimentation from volcaniclastics to carbonates was provided in the northern shelf of the Neotethys. Approximately 15–20 m.yr. later, following carbonate deposition, slab breakoff occurred. This event supplied suitable conditions for the generation of magmatic rocks possessing collisional signatures (subduction related and intraplate type) and caused epirogenic movements recorded by disconformities and deposition of clastic sediments in the backarc basin.

ACKNOWLEDGMENTS

This research was supported by the Research Foundation of Karadeniz Technical University (2007 .118.002.2 and 2009.112-005-2). E. Reitter is thanked for his help during the Sr-Nd-Pb isotope analyses. We wish to thank the reviewer, D. van Hinsbergen, and Editor D. Rowley, who provided many comments that improved the manuscript. We also wish to remember the sixth author of this essay, Ahmet Sami Derman, who died on May 18, 2012. He enabled us to become aware of the mafic rocks in this study during the fieldwork for his project on the Upper Jurassic–Lower Cretaceous carbonates of the Eastern Pontides.

REFERENCES CITED

Adamia, S.; Alania, V.; Chabukiani, A.; Kutelia, Z.; and Sadradze, N. 2011. Great Caucasus (Cavcasioni): a long-lived north-Tethyan back-arc basin. Turk. J. Earth Sci. 20:611–628.

Adamia, S. A.; Lordkipanidze, M. B.; and Zakariadze, G. S. 1977. Evolution of an active continental margin as exemplified by the alpine history of the Caucasus. Tectonophysics 40:183–199.

Akdoğan, R.; Turan, M.; and Dokuz, A. 2012. Geochemical properties and provenance characteristics of the Early-Middle Jurassic sandstone and shales, NE Turkey. EGU Gen. Assem. Conf. Abstr. 14:12004.

Arslan, M.; Temizel, İ.; Abdioğlu, E.; Kolaylı, H.; Yücel, C.; Boztuğ, D.; and Şen, C. 2013. ^{40}Ar-^{39}Ar dating, whole-rock and Sr-Nd-Pb isotope geochemistry of post-collisional Eocene volcanic rocks in the southern part of the Eastern Pontides (NE Turkey): implications for magma evolution in extension-induced origin. Contrib. Mineral. Petrol. 166:113–142.

Aydın, F. 2014. Geochronology, geochemistry, and petrogenesis of the Macka subvolcanic intrusions: implications for the Late Cretaceous magmatic and geodynamic evolution of the eastern part of the Sakarya Zone, northeastern Turkey. Int. Geol. Rev. 56:1246–1275.

Aydınçakır, E. 2014. The petrogenesis of Early Eocene non-adakitic volcanism in NE Turkey: constraints on the geodynamic implications. Lithos 208:361–377.

Aydınçakır, E., and Şen, C. 2013. Petrogenesis of the post-collisional volcanic rocks from the Borçka (Artvin) area: implications for the evolution of the Eocene magmatism in the Eastern Pontides. Lithos 172:98–117.

Barbarin, B. 1999. A review of the relationships between granitoid types, their origins and their geodynamic environments. Lithos 46:605–626.

Bowen, N. L. 1928. The evolution of the igneous rocks. Princeton, NJ, Princeton University Press, x + 334 p. Reprinted with a new introduction by J. F. Schairer and a complete bibliography of the writings of N. L. Bowen, Dover Publications, New York, 1956.

Bozkuş, C. 1992. Olur (Erzurum) yöresinin stratigrafisi. Geol. Bull. Turk. 35:103–119 (in Turkish with English abstract).

Carmichael, I. S. E. 1964. The petrology of Thingmuli, a Tertiary volcano in eastern Iceland. J. Petrol. 5:435–460.

Davies, J. H., and von Blackenburg, F. 1995. Slab breakoff: a model of lithospheric detachment and its test in the magmatism and deformation of collisional orogens. Earth Planet. Sci. Lett. 129:85–102.

Delaloye, M., and Bingol, E. 2000. Granitoids from western and northwestern Anatolia: geochemistry and modelling of geodynamic evolution. Int. Geol. Rev. 42:241–268.

Dokuz, A. 2000. Yusufeli (Artvin-Turkey) yöresinin jeolojisi, jeotektoniği, magmatik-metamorfik kayaçların jeokimyası ve petrojenezi. PhD thesis, Karadeniz Teknik Üniversitesi, Trabzon (in Turkish with English abstract).

———. 2011. A slab detachment and delamination model for the generation of Carboniferous high-potassium I-type magmatism in the Eastern Pontides, NE Turkey: the Köse composite pluton. Gondwana Res. 19:926–944.

Dokuz, A.; Karslı, O.; Chen, B.; and Uysal, İ. 2010. Sources and petrogenesis of Jurassic granitoids in the Yusufeli area, northeastern Turkey: implications for pre- and post-collisional lithospheric thinning of the Eastern Pontides. Tectonophysics 480:259–279.

Dokuz, A., and Tanyolu, E. 2006. Geochemical constraints on the provenance, mineral sorting and subaerial weathering of Lower Jurassic and Upper Cretaceous clastic rocks from the Eastern Pontides, Yusufeli (Artvin), NE Turkey. Turk. J. Earth Sci. 15:181–209.

Dokuz, A.; Tanyolu, E.; and Genç, S. 2006. A mantle- and a lower crust–derived bimodal suite in the Yusufeli (Artvin) area, NE Turkey: trace element and REE evidence for subduction-related rift origin of Early Jurassic Demirkent intrusive complex. Int. J. Earth Sci. 95: 370–394.

Dokuz, A.; Uysal, İ.; Dilek, Y.; Karslı, O.; Meisel, T.; and Kandemir, R. 2015. Geochemistry, Re-Os isotopes and highly siderophile element abundances in the Eastern Pontide peridotites (NE Turkey): multiple episodes of melt extraction-depletion, melt-rock interaction and fertilization of the Rheic Ocean mantle. Gondwana Res. 27:612–628.

Dokuz, A.; Uysal, İ.; Kaliwoda, M.; Karslı, O.; Ottley, C. J.; and Kandemir, R. 2011. Early abyssal and late SSZ-type vestiges of the Rheic oceanic mantle in the Variscan basement of the Sakarya Zone, NE Turkey: implications for the sense of subduction and opening of the Paleotethys. Lithos 127:176–191.

Dokuz, A.; Uysal, İ.; Meisel, W.; Turan, M.; Duncan, R.; and Akçay, M. 2013. Post-collisional adakitic volcanism in the eastern part of the Sakarya Zone, Turkey: evidence for slab and crustal melting. Contrib. Mineral. Petrol. 166:1443–1468.

Duchesne, J. C.; Shumlyanskyy, L.; and Charlier, B. 2006. The Fedorivka layered intrusion (Korosten Pluton, Ukraine): an example of highly differentiated ferrobasaltic evolution. Lithos 89:353–376.

Duggen, S.; Hoernle, K.; Bogaard, P.; and Garbe-Schonberg, D. 2005. Post-collisional transition from subduction- to intraplate-type magmatism in the westernmost Mediterranean: evidence for continental-edge delamination of subcontinental lithosphere. J. Petrol. 46:1155–1201.

Edwards, C. M. H.; Menzies, M. A.; Thirlwall, M. F.; Morris, J. D.; Leeman, W. P.; and Harmon, R. S. 1994. The transition to potassic alkaline volcanism in island arcs: the Ringgit-Beser complex, East Java, Indonesia. J. Petrol. 35:1557–1595.

Elliot, T.; Plank, T.; Zindler, A.; White, W. M.; and Bourdon, B. 1997. Element transport from subducted slab to juvenile crust at the Mariana arc. J. Geophys. Res. 102:14,991–15,019.

Erlank, A. J.; Hawkesworth, C. J.; Haggerty, S. E.; Allsopp, H. L.; Rickard, R. S.; and Menzies, M. A. 1987. Evidence for mantle metasomatism in peridotite nodules of the Kimberley pipes, South Africa. *In* Hawkesworth, C. J., and Menzies, M., eds. Mantle metasomatism. New York, Academic Press, p. 221–331.

Evcimen, E.; Duygu, L.; Tunçdemir, V.; Erdem, Y.; Yurteri, C.; Bakırhan, B.; Karslı, O.; Kandemir, R.; and Dokuz, A. 2014. Stratigraphic features of the area between Çamlıhemşin (Rize)–İspir (Erzurum)–Yusufeli (Artvin) arasında kalan alanın stratigrafik özellikleri. 67th Geological Congress of Turkey, Ankara, 69 p.

Eyüboğlu, Y.; Dilek, Y.; Bozkurt, E.; Bektaş, O.; Rojay, B.; and Şen, C. 2010. Structure and geochemistry of an Alaskan-type ultramafic-mafic complex in the Eastern Pontides, NE Turkey. Gondwana Res. 18:230–252.

Eyüboğlu, Y.; Santosh, M.; and Chung, S. L. 2011. Crystal fractionation of adakitic magmas in the crust-mantle transition zone: petrology, geochemistry and U-Pb zircon chronology of the Seme adakites, Eastern Pontides, NE Turkey. Lithos 121:151–166.

Fenner, C. N. 1929. The crystallization of basalt. Am. J. Sci. 18:223–253.

Fitton, J. G.; James, D.; and Leeman, W. P. 1991. Basic magmatism associated with the late Cenozoic extension in the western United States: compositional variations in space and time. J. Geophys. Res. 96: 13,693–13,711.

Foley, S. F.; Jackson, S. E.; Fryer, B. J.; Greenouch, J. D.; and Jenner, G. A. 1996. Trace element partition coefficients for clinopyroxene and phlogopite in an alkaline lamprophyre from Newfoundland by LAM-ICP-MS. Geochim. Cosmochim. Acta 60:629–638.

Furman, T., and Graham, D. 1999. Erosion of lithospheric mantle beneath the East African Rift system: geochemical evidence from the Kivu volcanic province. Lithos 48:237–262.

Hofmann, A. W.; Jochum, K. P.; Seufert, M.; and White, W. M. 1986. Nb and Pb in oceanic basalts: new constraints on mantle evolution. Earth Planet. Sci. Lett. 79:33–45.

Genç, Ş. C., and Tüysüz, O. 2010. Tectonic setting of the Jurassic bimodal magmatism in the Sakarya Zone (Central and Western Pontides), northern Turkey: a geochemical and isotopic approach. Lithos 118:95–111.

Golonka, J. 2004. Plate tectonic evolution of the southern margin of Eurasia in the Mesozoic and Cenozoic. Tectonophysics 381:235–273.

Göncüoğlu, M. C.; Turhan, N.; and Tekin, K. 2003. Evidence for the Triassic rifting and opening of the Neotethyan Izmir–Ankara Ocean and discussion on the presence of Cimmerian events at the northern edge of the Tauride-Anatolide Platform, Turkey. Boll. Soc. Geol. Ital. Spec. Publ. 2:203–212.

Görür, N.; Şengör, A. M. C.; Akkök, R.; and Yılmaz, Y. 1983. Pontidler'de Neotetis'in kuzey kolunun açılmasına ilişkin sedimantolojik veriler. Turk. Jeol. Kurumu Bülteni 26:11–20 (in Turkish with English abstract).

Green, T., and Pearson, N. 1987. An experimental study of Nb and Ta partitioning between Ti-rich minerals and silicate liquids at high pressure and temperature. Geochim. Cosmochim. Acta 51:55–62.

Harris, N. B. W.; Pearce, J. A.; and Tindle, A. G. 1986. Geochemical characteristics of collision zone magmatism. *In* Coward, M. P., and Ries, A. C., eds. Collision tectonics. Geol. Soc. Lond. Spec. Publ. 19:67–81.

Hart, S. R. 1984. A large-scale isotope anomaly in the Southern Hemisphere mantle. Nature 309:753–757.

Hastie, A. R.; Kerr, A. C.; Pearce, J. A.; and Mitchell, S. F. 2007. Classification of altered volcanic island arc rocks using immobile trace elements: development of

the Th-Co discrimination diagram. J. Petrol. 48:2341–2357.
Hofmann, A. W.; Jochum, K. P.; Seufert, M.; and White, W. M. 1986. Nb and Pb in oceanic basalts: new constraints on mantle evolution. Earth Planet. Sci. Lett. 33:33–45.
Hooper, P. R. 2000. Chemical discrimination of Columbia River basalt flows. Geochemistry Geophysics Geosystem 1:1024. doi:10.1029/2000GC000040.
Ionov, D. A.; Griffin, W. L.; and O'Reilly S. Y. 1997. Volatile bearing minerals and lithophile trace elements in the upper mantle. Chem. Geol. 141:153–184.
Jang, Y. D.; Naslund, H. R.; and McBirney, A. R. 2001. The differentiation trend of the Skaergaard intrusion and the timing of magnetite crystallisation: iron enrichment revisited. Earth Planet. Sci. Lett. 189:189–196.
Kandemir, R. 2004. Gümüşhane yakın yörelerindeki Erken-Orta Jura Yaşlı Şenköy Formasyonu'nun Çökel Özellikleri ve Birikim Koşulları. PhD thesis, Karadeniz Teknik Üniversitesi Fen Bilimleri Enstitüsü (In Turkish with English abstract).
Kandemir, R., and Lerosey-Aubril, R. 2011. First report of a trilobite in the Carboniferous of Eastern Pontides, NE Turkey. Turk. J. Earth Sci. 20:179–183.
Kandemir, R., and Yılmaz, C. 2009. Lithostratigraphy, facies, and deposition environment of the lower Jurassic Ammonitico Rosso type sediments (ARTS) in the Gümüşhane area, NE Turkey: implications for the opening of the northern branch of the Neo-Tethys Ocean. J. Asian Earth Sci. 34:586–598.
Karslı, O.; Chen, B.; Aydın, F.; and Şen, C. 2007. Geochemical and Sr-Nd-Pb isotopic compositions of the Eocene Dölek and Sariçiçek plutons, eastern Turkey: implications for magma interaction in the genesis of high-K calc-alkaline granitoids in a post-collision extensional setting. Lithos 98:67–96.
Karslı, O.; Dokuz, A.; Kaliwoda, M.; Uysal, İ.; Aydın, F.; Kandemir, R.; and Fehr, K. T. 2014. Geochemical fingerprints of Late Triassic calc-alkaline lamprophyres from the Eastern Pontides, NE Turkey: a key to understanding lamprophyre formation in a subduction-related environment. Lithos 196:181–197.
Karslı, O.; Dokuz, A.; Uysal, İ.; Aydın, F.; Kandemir, R.; and Wijbrans, J. 2010*a*. Generation of the early Cenozoic adakitic volcanism by partial melting of mafic lower crust, eastern Turkey: implications for crustal thickening to delamination. Lithos 114:109–120.
———. 2010*b*. Relative contributions of crust and mantle to generation of Campanian high-K calc-alkaline I-type granitoids in a subduction setting, with special reference to the Harsit Pluton, eastern Turkey. Contrib. Mineral. Petrol. 160:467–487.
Kaygusuz, A.; Arslan, M.; Siebel, W.; Sipahi, F.; and Ilbeyli, N. 2012. Geochronological evidence and tectonic significance of Carboniferous magmatism in the southwest Trabzon area, Eastern Pontides, Turkey. Int. Geol. Rev. 54:1776–1800.
Kaygusuz, A., and Aydınçakır, E. 2009. Mineralogy, whole-rock and Sr-Nd isotope geochemistry of mafic microgranular enclaves in Cretaceous Dagbasi granitoids, Eastern Pontides, NE Turkey: evidence of magma mixing, mingling and chemical equilibration. Chem. Erde 69:247–277.
Kepezhinskas, P. K.; Defant, M. J.; and Drummond, M. S. 1996. Progressive enrichment of island arc mantle by melt-peridotite interaction inferred from Kamchatka xenoliths. Geochem. Cosmochim. Acta 60:1217–1229.
Kieffer, B.; Arndt, N.; Lapierre, H.; Bastien, F.; Bosch, D.; Pecher, A.; Yirgu, G.; et al. 2004. Flood and shield basalts from Ethiopia: magmas from the African superswell. J. Petrol. 45:793–834.
Koch, R.; Bucur, I.; Kırmacı, M. Z.; Eren, M.; and Taslı, K. 2008. Upper Jurassic and Lower Cretaceous carbonate rocks of the Berdiga Limestone—sedimentation on an onbound platform with volcanic and episodic siliciclastic influx. Biostratigraphy, facies and diagenesis (Kircaova, Kale-Gumushane area; NE Turkey). N. Jb. Geol. Palaont. Abh. 247:23–61.
Konak, N.; Hakyemez, Y.; Bilgiç, T.; Bilgin, Z. R.; Hepşen, N.; and Ercan, T. 2001. Kuzeydoğu Pontidler'in (Oltu-Olur-Şenkaya-Narman-Tortum-Uzundere-Yusufeli) Jeolojisi. Maden Tetkik ve Arama Genel Müdürlüğü Jeoloji Etüdleri Dairesi, Kütüphane No. 613 (in Turkish).
Le Bas, M. J.; Le Maitre, R. W.; Streckeisen, A.; and Zanettin, B. 1986. A chemical classification of volcanic rocks on the total alkali-silica diagram. J. Petrol. 24:745–750.
Lehnert, K.; Su, Y.; Langmuir, C. H.; Sarbas, B.; and Nohl, U. 2000. A global geochemical database structure for rocks. Geochem. Geophys. Geosyst. 1:1999GC000026.
Ma, L.; Jiang, S.-Y.; Hofmann, A. W.; Dai, B.-Z.; Hou, M.-L.; Zhao, K.-D.; Chen, L.-H.; Li, J.-W.; and Jiang, Y-H. 2014. Lithospheric and asthenospheric sources of lamprophyres in the Jiaodong Peninsula: a consequence of rapid lithospheric thinning beneath the North China Craton? Geochim. Cosmochim. Acta 124:250–271.
McDonough, W. F., and Sun, S. S. 1995. The composition of the earth. Chem. Geol. 120:223–253.
Mederer, J.; Moritz, R.; Ulianov, A.; and Chiaradia, M. 2013. Middle Jurassic to Cenozoic evolution of arc magmatism during Neotethys subduction and arc-continent collision in the Kapan Zone, southern Armenia. Lithos 177:61–78.
Meijers, M. J. M.; Vrouwe, B.; van Hinsbergen, D. J. J.; Kuiper, K. F.; Wijbrans, J.; Davies, G. R.; Stephenson, R. A.; Kaymakcı, N.; Matenco, L.; and Saintot, A. 2010. Jurassic arc volcanism on Crimea (Ukraine): implications for the paleo-subduction zone configuration of the Black Sea region. Lithos 119:412–426.
Natland, J. H., and Dick, H. J. B. 2001. Formation of the lower ocean crust and the crystallization of gabbroic cumulates at a very slowly spreading ridge. J. Volcanol. Geotherm. Res. 110:191–233.
Nikishin, A.; Ziegler, P.; Bolotov, S.; and Fokin, P. 2012. Late Palaeozoic to Cenozoic evolution of the Black Sea–Southern Eastern Europe region: a view from the Russian Platform. Turk. J. Earth Sci. 21:571–634.
Nzegge, O. M.; Satir, M.; Siebel, W.; and Taubald, H. 2006. Geochemical and isotopic constraints on the

genesis of the Late Palaeozoic Deliktas and Sivrikaya granites from the Kastamonu granitoid belt (Central Pontides, Turkey). N. Jahrb. Geol. Palaeontol. 183:27–40.

Okay, A. 2000. Was the Late Triassic orogeny in Turkey caused by the collision of an oceanic plateau? *In* Bozkurt, E.; Winchester, J. A.; and Piper, J. D., eds. Tectonics and magmatism in Turkey and the surrounding area. Geol. Soc. Lond. Spec. Publ. 173:25–42.

Okay, A., and Göncüoğlu, M. C. 2004. Karakaya Complex: a review of data and concepts. Turk. J. Earth Sci. 13:77–95.

Okay, A., and Leven, E. J. 1996. Stratigraphy and paleontology of the Upper Paleozoic sequences in the Pulur (Bayburt) region, Eastern Pontides. Turk. J. Earth Sci. 5:145–155.

Okay, A., and Nikishin, A. M. 2015. Tectonic evolution of the southern margin of Laurasia in the Black Sea region. Int. Geol. Rev. 57:1051–1076.

Okay, A., and Şahintürk, Ö. 1997. Geology of the Eastern Pontides. *In* Robinson, A. G., ed. Regional and petroleum geology of the Black Sea and surrounding region. Am. Assoc. Petrol. Geol. Mem. 68:291–311.

Okay, A.; Satir, M.; and Siebel, W. 2006. Pre-Alpide Palaeozoic and Mesozoic orogenic events in the eastern Mediterranean region. Geol. Soc. Lond. Mem. 32: 389–405.

Okay, A.; Sunal, G.; Tüysüz, O.; Sherlock, S.; Keskin, M.; and Kylander-Clark, A. R. C. 2014. Low-pressure–high-temperature metamorphism during extension in a Jurassic magmatic arc, Central Pontides, Turkey. J. Metamorph. Geol. 32:49–69.

Okay, A., and Tüysüz, O. 1999. Tethyan sutures of northern Turkey. *In* Durand, B.; Jolivet, L.; Horváth, F.; and Sérane, M., eds. The Mediterranean basins: tertiary extension within the Alpine orogen. Geol. Soc. Lond. Spec. Publ. 156:475–515.

Osborn, E. E. 1959. Role of oxygen pressure in the crystallisation and differentiation of basaltic magmas. Am. J. Sci. 257:609–647.

Pearce, J. A., and Norry, M. J. 1979. Petrogenetic implications of Ti, Zr, Y and Nb variations in volcanic rocks. Contrib. Mineral. Petrol. 69:33–47.

Peccerillo, A., and Taylor, S. R. 1976. Geochemistry of Eocene calc-alkaline volcanic rocks from Kastamonu area, northern Turkey. Contrib. Mineral. Petrol. 58:63–81.

Pelin, S. 1977. Alucra (Giresun) Güneydoğu Yöresinin Petrol Olanakları Bakımından İncelenmesi, Doç. Tezi. Karadeniz Teknik Üniversitesi Yer Bilimleri Fakültesi, No. 13, Trabzon, 115 p. (in Turkish).

Petrone, C. M.; Francalanci, L.; Carlson, R.; Ferrari, L.; and Conticelli, S. 2003. Unusual coexistence of subduction-related and intraplate-type magmatism: Sr, Nd and Pb isotope and trace element data from the magmatism of the San Pedro-Ceboruco graben (Nayarit, Mexico). Chem. Geol. 19:1–24. doi:10.1016/S0009-2541(02)00229-2.

Pickett, E. A., and Robertson, A. H. F. 2004. Significance of the volcanogenic Nilüfer Unit and related components of the Triassic Karakaya Complex for Tethyan subduction/accretion processes in NW Turkey. Turk. J. Earth Sci. 13:97–143.

Plank, T., and Langmuir, C. H. 1998. The chemical composition of subducting sediment and its consequences for the crust and mantle. Chem. Geol. 145:325–394.

Roberts, M. P., and Clemens, J. D. 1993. Origin of high-potassium, calcalkaline, I-type granitoids. Geology 21: 825–828.

Robertson, A. H. F.; Ustaömer, T.; Pickett, E. A.; Collins, A. S.; and Dixon, J. E. 2004. Testing models of Late Palaeozoic–Early Mesozoic orogeny in western Turkey: support for an evolving open-Tethys model. J. Geol. Soc. Lond. 161:501–511.

Saintot, A.; Brunet, M.-F.; Yakovlev, F.; Sébrier, M.; Stephenson, R.; Ershov, A.; Chalot-Prat, F.; and McCann, T. 2006. The Mesozoic-Cenozoic tectonic evolution of the Greater Caucasus. *In* Gee, D. G., and Stephenson, R. A., eds. European lithosphere dynamics. Geol. Soc. Lond. Mem. 32:277–289.

Saunders, A. D.; Storey, M.; Kent, R. W.; and Nory, M. J. 1992. Consequences of plume-lithosphere interactions. *In* Alabaster, T.; Storey, B. C.; and Pankhurst, R. J., eds. Magmatism and the causes of continental break-up. Geol. Soc. Lond. Spec. Publ. 68:41–60.

Schmidt, M.; Dardon, A.; Chazot, G.; and Vannucci, R. 2004. The dependence of Nb and Ta rutile-melt partitioning on melt composition and Nb/Ta fractionation during subduction processes. Earth Planet. Sci. Lett. 226:415–432.

Sims, K. W. W., and De Paolo, D. J. 1997. Inferences about mantle magma sources from incompatible element concentration ratios in oceanic basalts. Geochim. Cosmochim. Acta 61:765–784.

Şen, C. 2007. Jurassic volcanism in the Eastern Pontides: is it rift related or subduction related? Turk. J. Earth Sci. 16:523–539.

Şengör, A. M. C. 1984. The Cimmeride orogenic system and the tectonics of Eurasia. Geol. Soc. Am. Spec. Pap. 195.

Şengör, A. M. C.; Cin, A.; Rowley, D. B.; and Nie, S.-Y. 1993. Space-time patterns of magmatism along the Tethysides: a preliminary study. J. Geol. 101:51–84.

Şengör, A. M. C., and Yılmaz, Y. 1981. Tethyan evolution of Turkey: a plate tectonic approach. Tectonophysics 75:181–241.

Şengör, A. M. C.; Yılmaz, Y.; and Sungurlu, O. 1984. Tectonics of the Mediterranean Cimmerides: nature and evolution of the western termination of Paleotethys. *In* Dixon, J. E., and Robertson, A. H. F., eds. The geological evolution of the eastern Mediterranean. Geol. Soc. Lond. Spec. Publ. 17:77–112.

Sun, S. S. 1980. Lead isotopic study of young volcanic rocks from mid-ocean ridges, ocean islands and island arcs. Philos. Trans. R. Soc. Lond. Ser. A 297:409–445.

Sun, S. S., and McDonough, W. F. 1989. Chemical and isotopic systematics of oceanic basalts: implications for mantle composition and processes. *In* Saunders, A. D., and Norry, M. J., eds. Magmatism in the ocean basins. Geol. Soc. Lond. Spec. Publ. 42:313–346.

Taylor, S. R., and McLennan, S. M. 1985. The continental crust: its composition and evolution. Oxford, Blackwell Scientific, 312 p.

Toplis, M. J., and Carroll, M. R. 1995. An experimental study of the influence of oxygen fugacity on Fe-Ti oxide stability, phase relations and mineral-melt equilibra in ferro-basaltic systems. J. Petrol. 36:1137–1170.

Topuz, G.; Altherr, R.; Kalt, A.; Satir, M.; Werner, O.; and Schwarz, W. H. 2004. Aluminous granulites from the Pulur complex, NE Turkey: a case of partial melting, efficient melt extraction and crystallization. Lithos 72: 183–207.

Topuz, G.; Altherr, R.; Schwarz, W. H.; Dokuz, A.; and Meyer, H. P. 2007. Variscan amphibolite-facies rocks from the Kurtoğlu metamorphic complex, Gümüşhane area, Eastern Pontides, Turkey. Int. J. Earth Sci. 96:861–873.

Topuz, G.; Altherr, R.; Siebel, W.; Schwarz, W. H.; Zack, T.; Hasözbek, A.; Barth, M.; Satır, M.; and Şen, C. 2010. Carboniferous high-potassium I-type granitoid magmatism in the Eastern Pontides: the Gümüşhane pluton (NE Turkey). Lithos 116:92–110.

Topuz, G.; Göçmengil, G.; Rolland, Y.; Çelik, Ö. F.; Zack, T.; and Schmitt, A. K. 2013. Jurassic accretionary complex and ophiolite from northeast Turkey: no evidence for the Cimmerian continental ribbon. Geology 41:255–258.

Ustaömer, T., and Robertson, A. H. F. 2010. Late Palaeozoic–Early Cenozoic tectonic development of the Eastern Pontides (Artvin area), Turkey: stages of closure of Tethys along the southern margin of Eurasia. Geol. Soc. Lond. Spec. Publ. 340:281–327.

Ustaömer, T.; Robertson, A. H. F.; Ustaömer, P. A.; Gerdes, A.; and Peytcheva, I. 2013. Constraints on Variscan and Cimmerian magmatism and metamorphism in the Pontides (Yusufeli-Artvin area), NE Turkey from U-Pb dating and granite geochemistry. *In* Robertson, A. H. F.; Parlak, O.; and Ünlügenç, U.-C., eds. Geological development of Anatolia and the easternmost Mediterranean. Geol. Soc. Lond. Spec. Publ. 372:49–74.

van Hunen, J., and Allen, M. B. 2011. Continental collision and slab break-off: a comparison of 3-D numerical models with observations. Earth Planet. Sci. Lett. 302: 27–37.

Veklser, I. V. 2009. Extreme iron enrichment and liquid immiscibility in mafic intrusions: experimental evidence revisited. Lithos 111:72–82.

Weaver, B. L., and Tarney, J. 1984. Empirical approach to estimating the composition of the continental crust. Nature 310:575–577.

Wedepohl, K. H. 1995. The composition of the continental crust. Geochim. Cosmochim. Acta 59:1217–1232.

Woodhead, J. D.; Hergt, J. M.; Davidson, J. P.; and Eggins, S. M. 2001. Hafnium isotope evidence for "conservative" element mobility during subduction zone processes. Earth Planet. Sci. Lett. 192:331–346.

Xia, L.; Xia, Z.; Xu, X.; Li, X.; and Ma, Z. 2013. Late Paleoproterozoic rift-related magmatic rocks in the North China Craton: geological records of rifting in the Columbia supercontinent. Earth-Sci. Rev. 125:69–86.

Xu, Y. G.; Mei, H. J.; Xu, J. F.; Huang, X. L.; Wang, Y. J.; and Chuang, S. L. 2003. Origin of two differentiation trends in the Emeishan flood basalts. Chin. Sci. Bull. 48:390–394.

Yang, J.-H.; Sun, J.-F.; Chen, F.; Wilde, S. A.; and Wu, F.-Y. 2007. Sources and petrogenesis of Late Triassic dolerite dikes in the Liaodong Peninsula: implications for post-collisional lithosphere thinning of the eastern North China Craton. J. Petrol. 48:1973–1997.

Yılmaz, O., and Boztuğ, D. 1986. Kastamonu granitoid belt of northern Turkey: first arc plutonism product related to the subduction of the Paleo-Tethys. Geology 14:179–183.

Yılmaz, Y.; Tüysüz, O.; Yiğitbaş, E.; Genç, Ş. C.; and Şengör, A. M. C. 1997. Geology and tectonic evolution of the Pontides. *In* Robinson, A. G., ed. Regional and petroleum geology of the Black Sea and surrounding region. AAPG Mem. 68:183–226.

Zindler, A., and Hart, S. R. 1986. Chemical geodynamics. Annu. Rev. Earth Planet. Sci. 14:493–571.

Zou, H. B.; Zindler, A.; Xu, X. S.; and Qi, Q. 2000. Major, trace element, and Nd, Sr and Pb isotope studies of Cenozoic basalts in SE China: mantle sources, regional variations, and tectonic significance. Chem. Geol. 171:33–47.